Loss of ErbB3 redirects Integrin β1 from early endosomal recycling to secretion in extracellular vesicles

Dorival Mendes Rodrigues-Junior[#*1]; Ana Rosa Sáez-Ibáñez[#2]; Takeshi Terabayashi[3]; Nina Daubel[4]; Taija Mäkinen[4] Olof Idevall-Hagren[5]; Aristidis Moustakas[1]; Ingvar Ferby*[2,4]

[1]Department of Medical Biochemistry and Microbiology, Science for Life Laboratory, Box 582, Biomedical Center, Uppsala University, SE-751 23 Uppsala, Sweden

[2]Department of Medical Biochemistry and Microbiology, Box 582, Biomedical Center, Uppsala University, SE-751 23 Uppsala, Sweden

[3]Department of Pharmacology, Oita University, Faculty of Medicine, Oita, Japan

[4]Department of Immunology, Genetics and Pathology, Uppsala University, 751 85 Uppsala, Sweden

[5]Department of Medical Cell Biology, Uppsala University, 751 23 Uppsala, Sweden

*** Corresponding authors:** Ingvar Ferby, e-mail:ingvar.ferby@igp.uu.se; Dorival Mendes Rodrigues-Junior, dorival.mrj@imbim.uu.se

[#]These authors contributed equally

Running title: ErbB3 as a component of the endocytic machinery

Final character count (main text): 9526

ABSTRACT

Receptor tyrosine kinases (RTKs) are important cargo in endocytic trafficking, yet their role in endosomal sorting and maturation of multivesicular bodies (MVBs) remains unclear. Here we show that the ErbB3 receptor sorts internalised Integrin β1, and the transferrin receptor (TfR), for endocytic recycling, in a manner that does not require ligand-induced ErbB3 signaling in breast epithelial cells. Loss of ErbB3 abrogates recycling of Integrin β1, likely from a Rab4-positive compartment, and redirects it toward lysosomal degradation and secretion as extracellular vesicle (EV) cargo. ErbB3 depletion impairs the collective migration of breast epithelial cell sheets, coinciding with reduced cell surface levels of Integrin β1 and increased release of Integrin β1-containing EVs. In contrast, EVs secreted from ErbB3-depleted cells enhance the motility of wild-type cells. Mechanistically, ErbB3 promotes assembly of the Arf6–GGA3–Rabaptin5 endosomal sorting complex to facilitate early recycling and suppress EV release. These findings provoke the notion that pseudo-RTKs play an active role in vesicular trafficking.

40 **INTRODUCTION**

41 The epidermal growth factor receptor (EGFR) family of receptor tyrosine kinases (RTKs),
42 including EGFR, ErbB2, ErbB3 and ErbB4, form homo- or heterodimers and play key roles in
43 epithelial development and homeostasis while their deregulation contributes to most epithelial
44 cancers (Schlessinger et al. 2002). RTK dimers are activated upon ligand-binding, leading to
45 recruitment of molecules that initiate intracellular signaling cascades. ErbB3 has impaired
46 kinase activity, but signals by forming heterodimers with other members of the EGFR family,
47 and accumulating evidence highlights its potent oncogenic activity. In particular, ErbB3 has
48 been linked to the migratory behaviour and metastasis of cancer cells and is responsible for
49 acquired resistance to anti-EGFR therapies (Gaborit et al. 2016; Pradeep et al. 2014; Smirnova
50 et al. 2012; Yoshioka et al. 2010; Tiwary et al. 2014).

51 Ligand-binding to RTKs also triggers receptor internalisation and trafficking within the cells
52 which determines strength, duration and spatial distribution of EGFR signals (Al-Akhrass et al.
53 2017; Avraham et al. 2011; Miaczynska et al. 2010; Sorkin et al. 2009; Wiley et al. 2003).
54 RTKs, including EGFRs, are internalised through clathrin-dependent and -independent
55 mechanisms, converging on the delivery of the receptors to early endosomes (Sorkin et al.
56 2009). Notably, although the mechanisms regulating ErbB3 turnover are still not fully
57 understood, protein kinase C (PKC) has been linked promoting ErbB3 endosomal sorting
58 (Dietrich et al. 2019). Thereafter, RTKs are diverted towards either (i) the plasma membrane
59 via recycling; (ii) protein degradation through lysosomes; or (iii) secretion in the extracellular
60 milieu as cargo of small extracellular vesicles (EVs) (Fosdahl et al. 2017; van Niel et al. 2022).
61 The collective term EVs refers to a variety of secreted nanovesicles confined by a lipid bilayer,
62 such as (i) exosomes, which have endosomal origin, are formed upon the maturation of MVBs
63 and are released into the extracellular milieu or (ii) microvesicles originating from the plasma
64 membrane, both mediating intercellular communication from secreting to recipient cells by
65 carrying bioactive molecules (Raposo et al. 2013; van Niel et al. 2022).

66 Rab GTPases Rab4 ("short-loop") and Rab11 ("long-loop") are major regulators driving
67 endosomal trafficking and recycling of RTKs and other transmembrane proteins, including
68 Integrins (Bridgewater et al. 2012; Lolo et al. 2022; Tomas et al. 2014). Of note, the
69 ubiquitously expressed GGA1-3 proteins, which are clathrin adaptors dependent on small
70 GTPases of the Arf family, have been found to regulate Rab4- or -11-dependent endosomal
71 recycling of Integrin β1 (GGA2, GGA3), the Met and Ret RTKs (GGA3) and the Transferrin
72 receptor (TfR) (GGA1) (Arjonen et al. 2012; Crupi et al. 2020; Parachoniak et al. 2011;
73 Puertollano et al. 2004; Ratcliffe et al. 2016; Sahgal et al. 2019; Zhao et al. 2008). GGA
74 proteins contain several functional domains that bind to accessory proteins modulating
75 membrane trafficking, including Rabaptin5 (Puertollano et al. 2004; Mattera et al. 2003; Miller
76 et al. 2003; Zhai et al. 2003; Zhu et al. 2004). Rabaptin5 cooperatively promotes a linkage
77 among Rab5- and Rab4-containing microdomains on early endosomes to coordinate the
78 coupling of these domains, thereby regulating sorting of cargo including Integrin β3 and TfR
79 into recycling endosomes (Christodorides et al. 2012; de Renzis et al. 2002; Deneka et al.
80 2003; Pagano et al. 2004).

81 We found a novel role for ErbB3 in vesicular sorting whereby it stabilizes the Arf6-GGA3-
82 Rabaptin5 endosomal sorting complex, to promote early recycling of TfR and Integrin β1.
83 Depletion of ErbB3 or its effectors Rabaptin5 or GGA3 re-routes Integrin β1 from endocytic
84 recycling towards lysosomal degradation and secretion as EV cargo. Altogether, these findings
85 depict a novel mechanism by which a pseudo-RTK regulates endosomal events with potential
86 impact on endocytic pathway-related biomedicine.

87

88 **RESULTS**

89 **ErbB3 guides Integrin β1 to the leading edge of motile epithelial cell sheets**

90 ErbB3 (HER3) is commonly overexpressed in several types of cancer, contributing to tumor
91 progression and dissemination proposedly by promoting cell migration, yet the underlying

92 molecular mechanism and cellular function remain poorly understood likely due to its lack of
93 intrinsic kinase activity. To better elucidate the role of ErbB3 in cell migration, we assessed the
94 impact of ErbB3 silencing on migrating sheets of non-malignant breast epithelial MCF10A
95 cells. Depletion of ErbB3 in MCF10A cells (Figure 1A) reduced the rate of wound closure
96 compared to control (Figures 1B, C), with area under curve (AUC) increasing by 50.2% and
97 48.2% in DMSO vs. lapatinib-treated samples respectively (Figure 1D). Lapatinib is a dual
98 specificity EGFR/ErbB2 inhibitor that was administered to eliminate potential influence of EGF-
99 induced cell migration (Lauand et al. 2013; Maretzky et al. 2011). At the applied concentration
100 of 1μM, no cytotoxic effects were observed, while activation-linked phosphorylation of EGFR
101 and downstream ERK1/2 signaling was effectively blocked (Supplementary Figures S1A, B).
102 Additionally, the cell proliferation determined by EdU incorporation did not differ between
103 control or ErbB3 siRNA-transfected cells (Figure 1E). Thus, in the absence of any impaired
104 proliferation, the observed sheet migration defect caused by ErbB3 loss cannot be attributed
105 to reduced cell proliferation. Our data show that ErbB3 promotes migration of epithelial sheets
106 in a manner that does not require canonical transphosphorylation of ErbB3 by EGFR or ErbB2
107 or the kinase activity of these receptors.

108 Integrins are pivotal molecules regulating cell-cell adhesion and cell-extracellular matrix (ECM)
109 interactions and the β1 subunit is the most common among the 18 α and 8 β subunits, forming
110 the basis for cell survival and motility of epithelial (Sun et al. 2023; Weaver et al. 1997).
111 Endocytic recycling is important for the polarised and dynamic distribution of Integrins in
112 migrating cells (Haskins et al. 2014; Nader et al. 2016; Qu et al. 2016; Wali et al. 2014). Integrin
113 β1 localizes to the leading edge of migrating epithelial cells in a Rab4-dependent manner
114 (Arjonen et al. 2013; Ratcliffe et al. 2016). To evaluate whether ErbB3 regulates the distribution
115 of recycled Integrin β1 in sheets of migrating breast epithelia, a scratch wound was inflicted on
116 confluent monolayers of MCF10A cells, followed by their incubation for surface labelling with
117 Alexa488-conjugated Integrin β1 antibody for 1 hour on ice, prior to removal of the antibody
118 and subsequent incubation at 37°C for 1 hour (Figure 1F). Chased Integrin β1 and F-actin

119 were visualized in cells at the leading front of the closing cell-sheets by immunofluorescence
120 imaging (Figure 1G). Integrin β1 enrichment at the leading edge, or along cell-cell contacts
121 relative to adjacent cytoplasm was quantified in cells bordering the wound (boxed regions in
122 Figure 1G). RNAi-mediated depletion of ErbB3 led to a 59.6% decrease in Integrin β1
123 enrichment at the leading edge, as compared with control siRNA-treated cells after 1 hour of
124 tracing at 37°C (Figure 1H). At cell-cell contacts, Integrin β1 enrichment decreased by 42.5%
125 (Figure 1I). These results are consistent with a ligand-independent role of ErbB3 in recycling
126 Integrin β1 to the leading edge of migrating cells and to a lesser extent to cell-cell contacts.

127

128 **ErbB3 promotes endocytic recycling of Integrin β1**

129 Notably, ErbB3, like integrin β1, has been found to continuously endocytose and recycle back
130 to the plasma membrane in a manner that does not require ligand stimulation or other members
131 of the EGFR family (Fosdahl et al. 2017; Sak et al. 2012). Thus, we wondered whether
132 endosomal trafficking of ErbB3 might be coordinated with, or even regulate, endocytic sorting
133 and trafficking of Integrin β1. As an initial step, we asked whether ErbB3 colocalises with
134 internalised Integrin β1. Briefly, the surface pool of Integrin β1 on the luminal breast cancer
135 (BRCA) cell line, MCF7, was labelled on ice with an Alexa488-conjugated antibody, and
136 allowed to internalise for 15 minutes at 37°C, prior to fixation and immunolabelling of
137 endogenous ErbB3. MCF7 cells were used since they overexpress ErbB3 facilitating detection
138 of endogenous protein by immunofluorescence (Supplementary Figure S1C). Confocal
139 microscopy showed that ErbB3 and traced Integrin β1 colocalised on intracellular structures
140 likely to be endosomes based on their estimated size (0.5-2 μm), as well as in filopodia (Figures
141 2A-C). The degree of colocalisation on putative endosomes was determined from
142 deconvoluted confocal images by measuring enrichment of Integrin β1 on ErbB3-positive
143 putative endosomes, relative to their adjacent surrounding cytoplasm (Figure 2C). A significant
144 proportion, 32%, of the ErbB3-positive endosomal structures showed prominent Integrin β1
145 enrichment (>100%) (Figure 2D). Furthermore, traced surface labelled ErbB3 and Integrin β1

146 partially colocalised with EHD1, a marker of recycling endosomes, at the endogenous level
147 (Supplementary Figure S1D), consistent with co-ordinated trafficking of the two.

148 We next investigated the putative role of ErbB3 in endocytic trafficking of Integrin β1 by
149 conducting a recycling assay in MCF10A and in primary breast epithelial cells HMEC
150 (prHMEC) cells, as outlined in Figure 2E. Briefly, the cell-surface pools of Integrin β1 were
151 labelled with Alexa488-conjugated antibody on ice, prior to 15-minute incubation at 37°C, time
152 during which the internalised Integrins accumulate primarily in early endosomes (Roberts et
153 al. 2001). The proportion of surface-labelling Integrin antibody that remained on the cell surface
154 was then quenched with an anti-Alexa488 antibody on ice, as previously described (Arjonen
155 et al. 2012). Cells were subsequently incubated at 37°C and re-emergence of internalised
156 Integrin β1 at the basal membrane was followed by live cell TIRF microscopy imaging. About
157 70% of the chased Integrin β1 was detected at the plasma membrane already after 10 minutes
158 and ErbB3 silencing, using two independent and validated siRNAs reduced recycling of
159 Integrin β1 by 40-50% (Figures 2F, G; Supplementary Figures S1E, F). Similar results were
160 obtained on prHMEC cells (Figures 2H, I; Supplementary Figures S1G, H). The initial amount
161 of fluorophore-labelled Integrin β1 detected on the cell surface, prior to tracing, was 18-19%
162 lower upon ErbB3 knockdown when compared with MCF10A control (Supplementary Figures
163 S1I, J), but unchanged in prHMEC (Supplementary Figures S1K, L), as determined by confocal
164 imaging. Notably, Integrin β1 protein levels did not change significantly upon ErbB3 depletion
165 in MCF10A (Supplementary Figure S2A) and prHMEC cells (Supplementary Figure S2B), yet
166 ErbB3 ablation significantly increased *ITGB1* mRNA levels in MCF10A cells (Supplementary
167 Figure S2C).

168 The ErbB3 pseudo receptor is currently thought to exclusively act in a dimer configuration with
169 other members of the ErbB family. Thus, in order to determine whether its preferred
170 dimerization partners EGFR or ErbB2 play a part in endocytic recycling of Integrin β1 alongside
171 ErbB3, we subjected MCF10A cells to RNAi-mediated depletion of EGFR or ErbB2 prior to
172 assaying endocytic recycling of Integrin β1. Depletion of EGFR or ErbB2 did not impair Integrin

173 β1 recycling (Figures 2J, K; Supplementary Figures S2A, E-H), suggesting that ErbB3 acts
174 independently of its canonical heterodimer partners to promote endocytic recycling of Integrin
175 β1. Of note, ectopic expression of siRNA-resistant ErbB3 restored the surface pool of traced
176 surface-labelled Integrin β1 in ErbB3-depleted MCF10A cells, as visualized by confocal
177 imaging (Supplementary Figures S2I, J), indicating that off-target effects of the ErbB3 siRNA
178 does not underlie the observed recycling defect. Both EGFR and ErbB2 were expressed at
179 levels comparable to ErbB3 in MCF10A cells (Supplementary Figure S2A). In contrast, ErbB4
180 was excluded from these experiments due to the lack of its expression in these cells, as
181 previously reported (Haskins et al. 2014; Wali et al. 2014). Of importance, the recycling assays
182 were conducted in a cell culture medium devoid of growth factors. Under these conditions we
183 did not detect tyrosine phosphorylation of immunoprecipitated ErbB3 by immunoblotting with
184 an antibody that recognises global phosphotyrosine (Supplementary Figure S2K), nor did we
185 detect phosphorylation of ErbB3 on Tyr1289, or significant activation of the AKT and ERK1/2
186 kinases, typically observed downstream of ligand-stimulated ErbB3 (Supplementary Figure
187 S2A). These results indicate that ErbB3 promotes Integrin β1 recycling in a manner that does
188 not require ligand-induced receptor signaling.

189 The finding that ErbB3 regulates endocytic recycling of Integrin β1 in non-malignant breast
190 epithelial cells raises the question of whether this mechanism is also relevant in cancer cells
191 overexpressing ErbB3. *ErbB3* mRNA is highly expressed in BRCA patients in comparison to
192 healthy controls (extracted from TCGA datasets; Supplementary Figure S3A), which correlates
193 significantly with a poorer overall survival of BRCA patients (Supplementary Figure S3B).
194 Moreover, higher mRNA levels of *ErbB3* were associated with the lack of response of BRCA
195 patients to chemotherapies (Supplementary Figure S3C), which is consistent with the known
196 pro-tumorigenic role of ErbB3 in BRCA (Pradeep et al. 2014; Smirnova et al. 2012; Tiwary et
197 al. 2014; Yoshioka et al. 2010; Gaborit et al. 2016). Notably, a meta-analysis of 12 studies
198 found that elevated ErbB3 protein expression was associated with worse overall survival not
199 only in BRCA patients, but also in patients with colorectal, gastric, melanoma, ovarian, head

200 and neck, pancreatic and cervical cancers (Ocana et al. 2013). Accordingly, we found *ErbB3*
201 mRNA levels significantly higher in the luminal BRCA cell line, MCF7, when compared to the
202 non-malignant breast epithelial cells MCF10A and the prHMEC (Supplementary Figure S1C).
203 To assess the putative role of ErbB3 in Integrin β1 recycling in malignant MCF7 cells we
204 surface-labelled Integrin β1 on ice, allowed internalisation at 37°C, followed by quenching of
205 the remaining surface labelling and subsequent tracing of internalised Integrin β1 in siCtrl or
206 siErbB3 cells, in line with our prior recycling assays. We found that Integrin β1 internalisation
207 was less effective in MCF7 cells as compared to MCF10A and prHMEC with limited detectable
208 return of internalised Integrin β1 to the cell surface of both control or ErbB3-depleted cells,
209 precluding reliable assessment of Integrin β1 recycling in these cells (Supplementary Figures
210 S3D, E). This observation may reflect differing Integrin β1 trafficking dynamics and underlying
211 mechanisms between malignant and normal breast epithelial cells.

212 Notwithstanding, we asked whether ErbB3 plays a more general role in regulating endosomal
213 recycling beyond Integrin β1, by assessing the effect of ErbB3-depletion on recycling of the
214 transferrin receptor (TfR) that has been extensively studied as a generic recycling cargo that
215 undergoes continuous internalisation and recycling with negligible sorting to late endosomes
216 and lysosomes (Sönnichsen et al. 2000). TfR on the cell-surface of MCF7 transfected with
217 control siRNA (siCtrl) or siErbB3 (Supplementary Figure S3F) were tagged with Alexa594-
218 conjugated transferrin on ice for 30 minutes. Unbound, labelled transferrin was washed away
219 and cells were incubated at 37°C in the presence of unlabelled transferrin for up to 1 hour.
220 Cells were brought back on ice and subjected to low pH treatment to quench Alexa594 that
221 had returned to the cell surface, followed by visualisation of chased transferrin retained in
222 endosomes by fluorescence imaging (Figures 2L-N). After 1 hour at 37°C, most TfR was
223 recycled back to the plasma membrane as indicated by the shedding of labelled transferrin
224 from the cells. However, half of the chased transferrin was still retained in endosomes in cells
225 transfected with siErbB3 (Figures 2M, N). In conclusions ErbB3 promotes recycling of both
226 Integrin β1 and TfR, consistent with a general role for ErbB3 in regulating endocytic recycling.

227

228 **ErbB3 colocalises with Rab4-positive recycling endosomes and impairs extracellular**
229 **vesicle release**

230 Our data shows a marked reduction in Integrin β1 recycling in ErbB3-depleted cells already 10
231 minutes post onset of tracing (Figure 2), which corresponds to the reported peak time of
232 colocalisation of Rab4 with traced TfR, preceding Rab11 and TfR colocalisation that peaks at
233 30 minutes (Lindsay et al. 2002; Sönnichsen et al. 2000). To determine which recycling
234 compartment ErbB3 preferentially resides in, ErbB3-mCherry was co-expressed with either
235 GFP-Rab4 or GFP-Rab11 in MCF10A cells, followed by treatment with either primaquine (PQ),
236 an inhibitor of endocytic recycling (Arjonen et al. 2012; Woods et al. 2004), or vehicle alone for
237 10 minutes and subsequent visualisation of the proteins by confocal imaging (Figure 3A).
238 Colocalisation was analysed as enrichment of ErbB3 fluorescence in Rab4- or Rab11-positive
239 compartments (Figure 3B) or visualized as average intensity projections of all structures
240 (Figure 3C). A large majority of ErbB3-mCherry did not colocalise with GFP-Rab4 or GFP-
241 Rab11 positive structures in the absence of PQ-treatment. However, upon PQ-treatment for
242 10 minutes, ErbB3 enrichment in Rab4-positive structures increased 6.2-fold ($p=0.0003$), while
243 no significant enrichment was observed in Rab11-positive structures (Figure 3B). The
244 preferred ErbB3 colocalisation with Rab4-positive rather than Rab11-positive recycling
245 endosomes and requirement for ErbB3 for early endocytic recycling (within 10 minutes)
246 (Bridgewater et al. 2012; Tomas et al. 2014), suggest that ErbB3 is required for early Rab4-
247 dependent endocytic recycling, although its involvement in other Rab dependent pathways are
248 not excluded.

249 We next asked whether ErbB3 might play a broader role in regulating exocytic trafficking,
250 beyond its known involvement in endocytic recycling. Thus, we used a well-established system
251 to analyse exocytic trafficking from the endoplasmic reticulum (ER) using ectopically
252 expressed vesicular stomatitis virus, VSV-G-ts-GFP (Hirschberg et al. 1998). The temperature
253 sensitive form of VSV-G accumulates in the ER at 40°C and upon shift to 32°C, this protein

254 traffics via the trans-Golgi-network (TGN) to the cell surface (Figure 3D). Of note, ErbB3
255 silencing in MCF10A cells did not affect the amount of VSV-G that was transported from the
256 ER to the cell surface after 30 minutes, 1 or 2 hours at permissive temperature as monitored
257 by immunoblotting of isolated surface-biotinylated proteins (Figures 3E, F and Supplementary
258 Figure S4A). Immunoblotting against the transmembrane protein Muc1 on the isolated
259 biotinylated proteins controlled for equal sampling. To complement the surface-biotinylation
260 assay, traced VSV-G-ts-GFP was visualized by confocal imaging. In both siCtrl- or siErbB3-
261 transfected MCF10A cells, VSV-G-ts-GFP exhibited predominant localization in the ER at
262 40°C. Following the shift to 32°C, VSV-G-ts-GFP was first detected in the GM130^{+} TGN at 30
263 minutes and in the E-cadherin^{+} membrane compartment at 1 hour, in both control and ErbB3
264 siRNA-transfected cells (Supplementary Figure S4B), suggesting that ErbB3 does not impact
265 trafficking from the TGN to the plasma membrane.

266 Interestingly, Rab4 has been proposed to restrict exosome biogenesis by promoting early
267 endosomal recycling (Zhang et al. 2022). To elucidate whether impaired endocytic recycling
268 caused by loss of ErbB3 could also influence EV release, we isolated small EVs secreted from
269 MCF10A cells transfected or not with ErbB3 or non-targeting siRNAs (Figure 3G) by an
270 established protocol of tangential flow filtration, followed by immune-affinity selection of the
271 tetraspanin CD81, or by ultracentrifugation (UC) (Figure 3H) (Rodrigues-Junior et al. 2019;
272 Théry et al. 2006). EVs enriched in the vesicular secretome fraction (VSF) were visualized by
273 transmission electron microscopy (TEM), validating the presence of membrane-surrounded
274 nanoparticles of 75–200 nm in size and consistent with small EVs (Supplementary Fig S4C).
275 Nanoparticle tracking analysis (NTA) revealed that the number of secreted EVs increased
276 significantly in cells with ErbB3 silenced by two independent siRNAs, in comparison to siCtrl,
277 while the EV modal size was not affected (Figure 3I, Supplementary Figure S4D). Additionally,
278 at equal EV fraction sample volume enriched as VSF, CD81-EVs or UC EVs from ErbB3-
279 depleted cells, the expression of established EV markers, including the endosomal sorting
280 complexes required for transport (ESCRT)-associated molecules ALIX and TSG101 or the

281 tetraspanins CD81 and CD63 were increased (Figures 3J-L), validating the NTA results.
282 Similarly, ErbB3 loss in prHMEC cells (Supplementary Figure S4E) did not impact the modal
283 size of EVs, but significantly enhanced the EV release (Supplementary Figure S4F).
284 Furthermore, Rab4A silencing in MCF10A cells (Figure 3L) significantly increased EV
285 secretion (Figure 3M), which is in line with the previous findings of Zhang et al. (2022). These
286 results were also reproduced in MCF7 cells, since ErbB3 or Rab4A silencing (Supplementary
287 Figure S4G) significantly boosted EV secretion (Supplementary Figures S4H, I). Collectively,
288 our data reveal a novel role for ErbB3 in promoting early endocytic recycling of different cell
289 surface-derived receptors, and restricting EV secretion in breast epithelial cells.

290

291 **ErbB3 loss directs Integrin β1 for lysosomal degradation and secretion in extracellular**
292 **vesicles**

293 We sought to trace the fate of internalised Integrin β1 that fails to recycle back to the cell
294 surface in the absence of ErbB3. Towards this end, MCF10A cells were labelled with an
295 Alexa488-conjugated surface-binding Integrin β1 antibody on ice, followed by incubation at
296 37°C for 15 minutes to allow Integrin β1 internalisation and subsequent quenching on ice of
297 the Integrin β1 that remained on the cell surface (0 minute). Finally, the cells were returned to
298 37°C and the fate of the internalised pool of Integrin β1 was visualized by confocal fluorescence
299 microscopy for up to half an hour (Figures 4A, B). Already after 15 minutes of tracing, Integrin
300 β1 levels decreased by 42.4% in ErbB3-depleted cells at which time no significant change was
301 observed in cells transfected with siCtrl (Figures 4B, C). Notably, traced Integrin β1 levels were
302 somewhat reduced already at the onset of the tracing (0 minute) in ErbB3-depleted cells
303 compared to control cells (13.3%) (Figure 4C), which is probably due to accelerated Integrin
304 β1 turnover in ErbB3 depleted cells evident within the 15-minute internalisation step that
305 precedes quenching and the onset of tracing.

306 To further assess the impact of ErbB3 on Integrin β1 turnover, we subjected control or ErbB3
307 siRNA-transfected MCF10A cells to treatment with the protein synthesis inhibitor
308 cycloheximide (CHX; up to 8 hours) and monitored Integrin β1 levels by immunoblotting
309 (Supplementary Figures S5A, B). While Integrin β1 levels were slightly reduced for up to 8
310 hours in the presence of CHX in the control cells, their levels were significantly decreased by
311 72% after 8 hours of CHX treatment in ErbB3-depleted cells (Supplementary Figures S5A, B).
312 To evaluate directly Integrin β1 stability, we performed a pulse-chase analysis of Integrin β1
313 turnover. Control or ErbB3 siRNA-transfected MCF10A cells were labelled with ^{35}S-
314 methionine/cysteine for 1 hour, followed by chasing with un-labelled amino acids at 37°C.
315 Integrin β1 was subsequently immunoprecipitated and the protein-incorporated ^{35}S-label was
316 determined by radiography. The data show that cells transfected with two independent siRNAs
317 against ErbB3 exhibited a significantly accelerated Integrin β1 turnover (49% or 84%
318 decrease), compared to control cells (Figures 4D, E).

319 The Integrin β1 turnover is slow, yet, limited degradation of this protein has been found to occur
320 in the lysosomes (De Franceschi et al. 2015). To better characterize Integrin β1 turnover, we
321 traced surface-labelled Integrin β1 in control or ErbB3 siRNA-transfected MCF10A cells by
322 confocal fluorescence microscopy, in the presence or absence of chloroquine, which impairs
323 phagolysosomal fusion (Figure 4F). Chloroquine treatment caused traced Integrin β1 to
324 accumulate in cells bordering the migratory front of wounded monolayers of both wild type and
325 ErbB3-depleted cells (Figures 4G). Quantification of fluorescence intensity showed that while
326 the level of traced Integrin β1 was reduced in the ErbB3-depleted cells relative to siCtrl cells
327 (by 44.8%, $p<0.0001$), consistent with its increased turnover, chloroquine treatment
328 significantly restored traced Integrin β1 levels (Figure 4H). Our results indicate that elevated
329 Integrin β1 turnover caused by ErbB3-loss is in part due to increased lysosomal degradation.

330 It has been reported that EV-associated Integrins assist organotropic metastasis and in
331 particular Integrin β1 was found to be associated with increased tumor invasiveness and
332 metastatic potential of BRCA cells (Hoshino et al. 2015; Weaver et al. 1997). In this context,

333 we sought to assess whether the sorting of Integrin β1 into EVs could be affected by ErbB3
334 silencing. We found that siRNA-mediated depletion of ErbB3 in MCF10A cells (Supplementary
335 Figure S5C) increased the amount of UC EV-associated Integrin β1, as detected by
336 immunoblotting (Figure 4I). The prevalence of EVs in the UC samples were further validated
337 by the increased presence of ALIX and CD81, in addition to the absence of the Golgi marker
338 GM130 (Figure 4I), and membranous nanovesicles labelled with CD63-immuno-gold were
339 visualized by TEM (Figure 4J), attesting to the EV integrity. These results imply that the
340 increased turnover of Integrin β1 in ErbB3-silenced cells occurs due to both increased
341 shedding in EVs and lysosomal degradation.

342 We sought to validate that EVs could be involved in promoting viability or invasive properties
343 of the breast epithelial cells. We therefore stimulated transfected MCF10A cells with
344 normalized concentrations of VSF (1×10^9 nanoparticles/mL) derived from either siCtrl or
345 siErbB3 cells for 48 hours and assessed cell viability by PrestoBlue fluorescence or invasion
346 into ECM (Matrigel) for additional 16 hours. We found that equalised amounts of EVs from
347 either control or ErbB3-depleted cells to the same extent, modestly promoted cell viability in
348 the recipient cells (Figure 4K). Accordingly, ErbB3 absence reduced MCF10A motility in
349 comparison to siCtrl cells (Figures 1A-D and Figure 4L), whereas the EV pools substantially
350 enhanced not only the motility of recipient ErbB3-depleted cells, but also the recipient siCtrl
351 cells into a Matrigel matrix (Figure 4L). Together, our results indicate that while ErbB3-silenced
352 MCF10A cells exhibited lower motility, these cells are sensitive to external stimuli received
353 from the EV cargo that elevate invasive behaviour, while simultaneously releasing a larger
354 amount of EVs with enhanced motility properties to neighbouring wild-type cells. Furthermore,
355 to test if Integrin β1 was essential for promoting EV-induced invasive behaviour, WT MCF10A
356 cells were pre-treated with EVs in the presence of 5 μg/mL IgG or Integrin β1 blocking
357 monoclonal antibody (mAb; clone P4C10) for 48 hours prior to the transfer into ECM (Figure
358 4M). We found that blocking Integrin β1 significantly reduced invasiveness of the cells both in
359 the presence or absence of EVs derived from MCF10A (Figure 4M). Moreover, MCF10A cells

360 transfected with siCtrl or siErbB3 were both sensitive to the inhibitory action of P4C10. The
361 data is consistent with EV-derived Integrin β1 playing a role in promoting invasive behaviour
362 of the MCF10A cells, in line with its known functions (Sun et al. 2023; Weaver et al. 1997).

363

364 **ErbB3 promotes assembly of the Arf6-Rabaptin5-GGA3 sorting complex and stability of**
365 **Rabaptin5 and GGA3**

366 Interestingly, selected components of the endosomal machinery that could be implicated in the
367 Rab4-dependent early recycling of β Integrins such as ADP-ribosylation factor-binding protein
368 3 (also known as Golgi-associated gamma adaptin ear containing, GGA3) (Arjonen et al. 2012)
369 and Rab GTPase-binding effector protein 1 (Rabaptin5 or RABPT5) (Christoforides et al. 2012;
370 Mattera et al. 2003) co-localised with ErbB3 in MCF7 cells (Supplementary Figures S5D, E).
371 Thus, to explore whether ErbB3 could interact with these proteins, we immunoprecipitated
372 endogenous ErbB3 from MCF10A cell extracts and examined co-precipitates by
373 immunoblotting. We found that ErbB3 co-precipitated efficiently with both GGA3 and
374 Rabaptin5 at endogenous levels (Figure 5A) and the abundance of this complex was increased
375 after a 30-minute treatment with PQ, consistent with these proteins interacting in the recycling
376 compartment. Thus, GGA3 and Rabaptin5 are plausible effectors of ErbB3 in early recycling
377 endosomes.

378 GGA3 has been shown to interact with ADP-ribosylation factor 6 (Arf6) to drive recycling of
379 different transmembrane proteins (Parachoniak et al. 2011; Ratcliffe et al. 2016) and with
380 Rabaptin5 to regulate TGN cargo export and endosomal tethering/fusion events (Mattera et al.
381 2003; Miller et al. 2003). We therefore set out to determine the influence of ErbB3 on the Arf6-
382 GGA3-Rabaptin5 adaptor network (Supplementary Figure S5F). MCF10A cells were
383 transfected with control or ErbB3 siRNA, prior to treatment with PQ or vehicle alone for 10
384 minutes. Harvested cell lysates were subsequently subjected to Arf6 immunoprecipitation and
385 immunoblotting for bound GGA3 and Rabaptin5 (Figure 5B). The data revealed that loss of

386 ErbB3 indeed reduced the amount of GGA3 and Rabaptin5 associated with Arf6 both in the
387 absence and in the presence of PQ. Notably, PQ treatment of siCtrl cells led to a stronger
388 interaction of Arf6 with GGA3 and Rabaptin5 (Figure 5B). Of note, Rabaptin5 and GGA3
389 protein levels were reduced in ErbB3-depleted cells (Figure 5C), which could explain the
390 reduced interaction. Nevertheless, the lower protein levels of GGA3 and Rabaptin5 was not
391 due to their reduced transcription, as determined by RT-qPCR (Figure 5D), suggesting
392 reduced protein stability. This is supported by the observation that treatment of ErbB3-depleted
393 MCF10A cells with the proteasome-inhibitor MG132 partially restored GGA3 and Rabaptin5
394 protein levels (Supplementary Figure S5G). It is possible that reduced engagement of GGA3
395 and Rabaptin5 in a stable complex with ErbB3, underlies its proteasomal degradation.

396 Deepening the mechanistic analysis, we noticed that ErbB3 has a unique putative GGA3-
397 binding motif (DxxLL) in the activation loop of the pseudokinase domain, that is not found on
398 EGFR or ErbB2 (Figure 5E). The DxxLL motif constitutes a consensus binding site for VHS
399 domains found in GGA proteins. To test whether ErbB3 binds GGA3 via this motif, we mutated
400 the two conserved leucines in ErbB3 to alanine (LL866/7AA). GGA3 was overexpressed with
401 or without ErbB3 wildtype or the LL866/7AA mutant in HEK293T cells followed by
402 immunoprecipitation of ErbB3 and immunoblotting against GGA3 (Figure 5F). We found that
403 GGA3 co-immunoprecipitated with wild-type but not the LL866/7AA mutant ErbB3 (Figure 5F),
404 suggesting that ErbB3 interacts with the VHS domain of GGA3 (Figure 5E). Thus, we tested
405 the hypothesis that ErbB3 scaffolds the assembly of the Arf6-GGA3-Rabaptin5 complex by
406 ectopically expressing these proteins in HEK293T cells with or without wild-type or LL866/7AA
407 mutant ErbB3, followed by immunoprecipitation of Arf6 and immunoblotting analysis of
408 associated ErbB3, GGA3 and Rabaptin5. We found that GGA3 and Rabaptin5 co-precipitated
409 more efficiently with Arf6 in the presence of wild-type but not mutant (LL866/7AA) ErbB3
410 (Figure 5G). In agreement, we found that the ectopically expressed LL866/7AA mutant form of
411 mCherry-tagged ErbB3 co-localised with fewer internalised Integrin β1-positive structures
412 compared to the wild-type (WT) receptor (Figure 5H). In addition to its interaction with GGA3

413 and consistent with its proposed scaffolding role for ErbB3, we found that ErbB3 can directly
414 bind Rabaptin5 in vitro, as demonstrated by pull-down experiments using recombinant GST-
415 ErbB3 incubated with recombinant MBP-Rabaptin5 (Supplementary Figure S5H). Taken
416 together, our data suggest that ErbB3 acts as a scaffold that associates with both GGA3 and
417 Rabaptin5 to promote the assembly of the Arf6-GGA3-Rabaptin5 endosomal sorting complex.
418 In the absence of ErbB3, GGA3 and Rabaptin5 protein levels are reduced possibly as a
419 consequence of their release from this sorting complex.

420

421 **Rabaptin5 and GGA3 are effectors of ErbB3 in endosomal trafficking**

422 Previous studies revealed the critical importance of Rabaptin5 for directing Integrin β3 towards
423 Rab4-dependent recycling (Do et al. 2017; Christoforides et al. 2012), however the same has
424 not yet been demonstrated for Integrin β1. Thus, we traced surface-labelled Integrin β1 in
425 MCF10A cells transfected with either control or Rabaptin5 siRNA and visualized the re-
426 emergence of internalised Integrin β1 at the basal membrane by TIRF live cell imaging (Figure
427 6A). Depletion of Rabaptin5 caused a significant reduction in the rate and amount of Integrin
428 β1 that recycled back to the basal membrane (Figures 6B-D), quantified as a significant
429 decrease of 28.7% in AUC.

430 Furthermore, we examined the impact of Rabaptin5-depletion on Integrin β1 stability by pulse-
431 chase analysis of protein turnover. Control or Rabaptin5 siRNA-transfected MCF10A cells
432 were labelled with ^{35}S-methionine/cysteine for 1 hour, followed by chasing with unlabelled
433 amino acids at 37ºC. Integrin β1 was subsequently immunoprecipitated and the incorporated
434 ^{35}S-label was determined by autoradiography. The data shows that Rabaptin5-depleted cells
435 exhibited accelerated Integrin β1 turnover, with a significant 49% reduction in 9 hours when
436 compared to control-treated cells (Figures 6E, F). Likewise, previous work has shown that
437 siRNA-mediated silencing of GGA3 re-routes Integrin β1 from Rab4-dependent recycling
438 towards lysosomal degradation (Ratcliffe et al. 2016).

439 We next assessed the impact of Rabaptin5 or GGA3 on EV release. Thus, Rabaptin5
440 knockdown in MCF10A and MCF7 cells (Figure 6G and Supplementary Figure S5I), followed
441 by NTA, revealed a significant increase in release of small EVs without impairing the EVs'
442 modal size in comparison to siCtrl cells (Figure 6H and Supplementary Figure S5J), while TEM
443 confirmed the presence of membrane-surrounded nanovesicles in the enriched VSF (Figure
444 6I and Supplementary Figure S5K). Moreover, MCF10A cells transfected with siCtrl, siErbB3
445 or siGGA3 (Figure 6J and Supplementary Figure S5L) had their EVs enriched by UC and
446 characterized by NTA, indicating that GGA3 depletion enhanced significantly EV secretion in
447 comparison to the siCtrl cells (Figure 6K), similar to ErbB3-depletion (Figure 3). In line with this
448 finding, further analysis of different positive and negative EV markers by immunoblotting
449 showed enrichment of ALIX, TSG101 and Integrin β1 in the UC EV fraction upon ErbB3 or
450 GGA3 depletion, while the Golgi marker GM130 was absent (Figure 6L). Of note, the
451 morphology of these EVs was monitored by TEM (Figure 6M). Hence, loss of either GGA3 or
452 Rabaptin5 mimics the effect of loss of ErbB3 on endocytic trafficking of Integrin β1, consistent
453 with the hypothesis that GGA3 and Rabaptin5 are effectors of ErbB3 in promoting endosomal
454 recycling and impeding EV release.

455

456 **DISCUSSION**

457 We report that the RTK family protein ErbB3 promotes endocytic recycling of Integrin β1 and
458 TfR in a ligand-independent manner, as well as that ErbB3 restricts the release of EV-
459 associated Integrin β1 (Figure 7). Endocytic trafficking of RTKs provides critical spatial and
460 temporal control of the intracellular signaling events they trigger, which ultimately governs
461 cellular response. Hence, the mechanisms by which RTKs internalise and traffic within the cell
462 has been subject to intense scrutiny. While prevailing knowledge centres on RTKs as vesicular
463 passengers, our study provides a compelling example of an RTK family member playing an
464 integral role in the endocytic trafficking machinery per se.

465 RTK signaling is integrated at many levels with the regulation of endocytic trafficking of
466 Integrins (Caswell et al. 2009; Ivaska et al. 2011; Woods et al. 2004). Growth factor mediated
467 activation of AKT or protein kinase D (PKD) can regulate Integrin recycling by phosphorylating
468 proteins, such as ACAP1, an ARF6GAP or Rabaptin5 (Christoforides et al. 2012; Li et al.
469 2005). Conversely, several studies have shown that Integrins alter recycling of other receptors,
470 such as EGFR and vascular endothelial growth factor receptor (VEGFR2), further highlighting
471 the close coordination of Integrins with RTK trafficking (Caswell et al. 2008; Reynolds et al.
472 2009). We found that ErbB3 can promote endocytic recycling of Integrin β1 and TfR,
473 independently of canonical ErbB3-driven tyrosine kinase signaling. Intriguingly, EGFR has
474 been reported to function in a ligand-independent manner to scaffold an exocyst subcomplex
475 needed to assemble autophagosomes (Tan et al. 2015). This invites wider speculation that
476 'inactive' RTKs, as exemplified by EGFR and ErbB3, might play an instrumental role in
477 intracellular vesicular trafficking as scaffolding centres.

478 We show that ErbB3 interacts with both GGA3 (via its VHS domain) and Rabaptin5 to promote
479 assembly and stability of the Arf6-GGA3-Rabaptin5 endosomal sorting complex. GGA3 has
480 previously been reported to be required to sort multiple cargos, such as Integrin β1, c-Met and
481 c-Ret for Rab4-dependent recycling (Crupi et al. 2020; Parachoniak et al. 2011; Ratcliffe et al.
482 2016). It is therefore possible that ErbB3 drives recycling of not only Integrin β1 and TfR as
483 reported here, but of diverse cargo that depends on Arf6-GGA3, although this remains to be
484 addressed. Furthermore, loss of ErbB3 redirects Integrin β1 towards lysosomes for
485 degradation, mimicking loss of GGA3 that similarly redirects both Integrin β1 (Ratcliffe et al.
486 2016) and c-Met towards lysosomal degradation (Parachoniak et al. 2011), or Rabaptin5
487 depletion that we find similarly redirects trafficking of internalised Integrin β1 towards lysosomal
488 degradation. Taken together these results lead us to propose that ErbB3 engages into
489 endocytic recycling by promoting formation and stability of the Arf6-GGA3-Rabaptin5 vesicular
490 adaptor complex, in line with the emerging concept that pseudo-kinases have evolved to
491 acquire scaffolding functions.

492 In addition to this, it has been shown by others that Arf6 interacts with Phospholipase D2, to
493 promote synthesis of phosphatidic acid and thereby formation of syntenin-ALIX intraluminal
494 vesicles, which are later secreted as exosomes (Ghossoub et al. 2014). Likewise, ARF6
495 activation leads to the phosphorylation of myosin light chain (MLC) and actomyosin
496 contraction, which allows the vesicles to bud off from the membranes of cancer cells
497 (Muralidharan-Chari et al. 2009). Thus, since ErbB3 promotes the assembly of the Arf6-GGA3-
498 Rabaptin5 complex, we speculate that ErbB3 association with GGA3 could negatively control
499 EV release by retaining Arf6 at early endosomes, which could suppress the formation of Arf6-
500 PLD2-PA complexes, explaining the reduced EV secretion in breast epithelial cells, although
501 further studies are required to address this hypothesis more rigorously.

502 Activation of EGFR and ErbB2 involve formation of asymmetric kinase domain dimers,
503 whereby one kinase domain acts as an 'activator' and the other as a 'receiver', that becomes
504 activated (Jura et al. 2009; Littlefield et al. 2014). However, the ErbB3 pseudo-kinase domain
505 acts only as an activator while the receiver interface diverges in sequence from other ErbB
506 receptor family members and is not engaged in kinase domain dimerization (Jura et al. 2009).
507 Interestingly, GGA3 interacts with a DxxLL motif situated on the activation loop within the
508 dysfunctional catalytic site in the ErbB3 pseudokinase domain. This motif is not present in
509 other ErbB receptor family members, where the corresponding position is instead involved in
510 regulating kinase activity. It is tempting to speculate that the dysfunctional catalytic domain in
511 ErbB3 may have evolved a novel kinase-independent function in regulating endocytic
512 trafficking, perhaps shedding some light on the enigmatic nature of pseudokinases.

513 Previous studies have found that Integrin β1 can physically interact with EGFR and endocytose
514 together (Caswell et al. 2008; Yu et al. 2000). Although ErbB3 and Integrin β1 were partially
515 co-localised at focal adhesions, cell-cell contacts and recycling endosomes, we did not find
516 that ErbB3 depletion influenced Integrin β1 internalisation. Thus, it remains to be elucidated
517 whether ErbB3 and Integrin β1 associate during endocytosis. Notwithstanding, our results
518 suggest that ErbB3 encounters Integrin β1 in recycling endosomes, presumably at the step

519 when the cargo is sorted into Rab4-positive vesicles through engagement of the Arf6-GGA3-
520 Rabaptin5-complex. This is suggested by the observation that Integrin β1 and ErbB3
521 colocalisation was primarily observed upon treatment with the recycling inhibitor primaquine,
522 when ErbB3 is retained in a Rab4-positive compartment, which coincides with enhanced
523 binding of ErbB3 to GGA3 and Rabaptin5. This is in accordance with previous studies showing
524 that the sortilin-related receptor (SorLA) attenuates ErbB3 lysosomal degradation by retaining
525 ErbB3 within Rab4-positive recycling endosomes (Al-Akhrass et al. 2021). Additionally, GGA3
526 has been found to be enriched in Rab4-positive endosomes alongside endocytosed Met, with
527 significantly lower enrichment observed in Rab5-positive early endosomes (Parachoniak et al.
528 2011). Interestingly, we found that ErbB3 is required for rapid recycling of Integrin β1 in non-
529 malignant breast epithelial cells, but failed to demonstrate the same effect in malignant MCF7
530 cells. It is well established that Integrin trafficking is regulated by multiple context-dependent
531 mechanisms (Moreno-Layseca et al. 2019). Thus, it will be interesting to investigate whether
532 Integrin endosomal sorting mechanisms change upon malignant transformation.

533 The proposed role of ErbB3 in endosomal sorting of Integrin β1 and TfR and possibly other
534 cargo into recycling endosomes, postulates that ErbB3 frequently resides in the sorting
535 compartment independent of ligand-stimulation. In line with this prediction, ErbB3 has been
536 found to continuously endocytose and recycle back to the plasma membrane (Cao et al. 2007;
537 Fosdahl et al. 2017; Sak et al. 2012) independent of either ligand stimulation or other members
538 of the EGFR family (Sak et al. 2012). Intriguingly, dynamic availability of ErbB3 in vesicular
539 compartments may also be regulated independently of EGFR and ErbB2, since steady-state
540 protein levels of ErbB3, but not EGFR or ErbB2, are tightly controlled by ligand-independent
541 ubiquitination by the E3-ligase Nrdp1 that localizes in perinuclear membranes and targets
542 ErbB3 for proteasomal degradation (Diamonti et al. 2002; Qiu et al. 2002). Furthermore, we
543 found that ErbB3-dependent cell sheet migration also does not require EGF or other growth
544 factors to signal. It is however noteworthy to stress that growth factor-induced EGFR or ErbB2
545 signaling is well known to promote cell migration, and our data does not rule out or address

546 the possible ErbB3 cooperation with EGFR or ErbB2 to drive growth factor-induced cell motility.
547 In this manuscript, we focus entirely on the unexpected and growth factor-independent roles
548 of ErbB3, distinguishing our investigation from the frequently studied and complex growth
549 factor-induced cell signaling events.

550 Hence, our data points to ErbB3 regulating Integrin β1 delivery to the leading edge of migrating
551 sheets of epithelial cells, promoting their migration. Since several studies established that
552 Integrin recycling promotes cell migration and cancer cell invasiveness (Caswell et al. 2008;
553 Pellinen et al. 2006), we reveal a new perspective of how ErbB3 could mechanistically
554 contribute to cell dissemination in part by promoting Integrin recycling. Conversely, we
555 speculate that loss of ErbB3 could lead to increased dissemination of heterogeneous tumours
556 by increasing EVs release, with the potential to increase invasiveness of surrounding wild-type
557 or mutant cells. This is consistent with the findings of Luhtala et al. (2018), who identified low
558 ErbB3 expression as a prognostic biomarker for shorter recurrence-free survival in patients
559 with ErbB2-amplified breast cancer. Furthermore, reduced ErbB3 levels were associated with
560 clinically aggressive features, including positive lymph node status, larger tumor size, triple-
561 negative subtype, and basal-like phenotype (Luhtala et al., 2018). Yet, in what context either
562 gain or loss of ErbB3 might be contributing to carcinogenesis remains to be explored. Of note,
563 EVs carry multiple functional molecules and whether ErbB3 affects the sorting of selected
564 protein EV cargo remains to be addressed by proteomic studies. Yet, our study revealed that
565 the pseudo-kinase ErbB3 plays a role in the vesicular sorting machinery by promoting rapid
566 endosomal recycling of other cargo and impeding EV release. This invites the wider
567 speculation that other pseudo-RTKs may also have evolved scaffolding functions that might
568 play instrumental roles in vesicular trafficking.

569

570 **Acknowledgements**

We thank Marino Zerial, Lukas Huber and Martin Offterdinger for kindly providing cDNA constructs. We also thank Carl-Henrik Heldin for valuable discussion and for critically reading the manuscript. This research was supported by the Swedish Cancer Society, grants CAN2018/469, CAN2021/1506Pj01H and CAN2024/24/3580Pj01H (A.M.); the Swedish Research Council, grant 2018-02757 and 2023-02865 (A.M.), Lars Hierta Memorial Foundation, grant FO2024-0173 (D.M.R-Jr); O.E. och Edla Johanssons Vetenskapliga Stiftelsen (D.M.R-Jr); Stiftelsen Längmanska kulturfonden, grant BA25-1369 (D.M.R-Jr). The Sigurs and Elsa Golje Memorial Foundation (LA2025-0172) (D.M.R-Jr).

Author Contributions

D.M.R-Jr., A.R.S., T.T., O.I., T.M. and I.F. conceived and designed the experiments; D.M.R-Jr., A.R.S., J.S., O.I. and N.D. performed the experiments; D.M.R-Jr., A.R.S., O.I. N.D., A.M. and I.F. interpreted the results; D.M.R-Jr., A.R.S. and I.F. wrote the manuscript, with input from all authors.

Declaration of Interests

The authors declare no competing interests.

Data and materials availability

Further information and requests for resources and reagents should be directed to and will be fulfilled by the Lead Contacts, Ingvar Ferby (ingvar.ferby@igp.uu.se) and Dorival Mendes Rodrigues-Junior (dorival.mrj@imbim.uu.se). The plasmids generated in this study are available upon request.

595 **MATERIALS AND METHODS**

596

597 **Correlation analysis of gene expression**

598 *ErbB3* mRNA expression comparison in BRCA tumor versus normal samples was retrieved
599 from the GEPIA2 server (https://gepia2.cancer-pku.cn/) (Tang et al. 2019). BRCA patients
600 overall survival was acquired using the KM plotter database (KMplot) (Lánczky et al. 2021).
601 Correlation of *ErbB3* mRNA expression and chemotherapy response in BRCA patients was
602 conducted using the ROC Plotter database (http://www.rocplot.org) (Fekete et al. 2019). BRCA
603 patients were categorized as non- or responders to treatment, according to the relapse-free
604 survival status at five years post-surgery.

605

606 **Cell lines and treatments**

607 MCF10A (RRID:CVCL_0598) cells were cultured in DMEM/F12 (Gibco) supplemented with
608 glutamine (Sigma-Aldrich), 5% horse serum (Gibco), 20 ng/mL epidermal growth factor (EGF)
609 (Miltenyi Biotech), 0.5 mg/mL hydrocortisone, 100 ng/ml cholera toxin and 10 µg/mL insulin
610 (all from Sigma-Aldrich). Where indicated, a starvation medium lacking serum, insulin and EGF
611 was used. Primary human mammary epithelial cells (prHMEC; RRID:CVCL_0307) from Gibco
612 were cultured in HMEC ready medium (Invitrogen). MCF7 (RRID:CVCL_0031) cells were
613 cultured in EMEM supplemented with 0.01 mg/mL human recombinant insulin and 10% foetal
614 bovine serum (FBS). HEK293T (RRID:CVCL_0063) cells were cultured in DMEM (Sigma-
615 Aldrich) with 10% FBS (Gibco). Unless otherwise stated, the cell lines were purchased from
616 ATCC. Culture conditions were 5% CO_2 at 37°C. Cell line authentication barcodes were
617 purchased from Eurofins to confirm the cells' identity and absence of contamination.
618 The EGFR/ErbB2 inhibitor lapatinib was used at 1 µM (LC Laboratories) and was batch-tested
619 for efficiency; cycloheximide at 50 µM (from Sigma-Aldrich); chloroquine at 50 µM (#14774;
620 Cell Signaling); primaquine (PQ) at 0.5 mM (#160393; Sigma-Aldrich) for 10 or 30 minutes;
621 MG132 (Calbiochem) at 50 µM. In all cases, control cells were treated with vehicle alone
622 (DMSO, from Sigma-Aldrich) at the corresponding concentration.

623

624 **Transfections**

625 Cells were transfected with RNAiMAX (Invitrogen) according to the supplier's instructions. A
626 final concentration of 20 nM of the following siRNAs were used: siErbB3#1
627 (5'CAAUACCAGACACUGUACAAGCUCU53'); siErbB3#2
628 (5'UCGUCAUGUUGAACUAUAA3'); siRab4A (5'GAACGAUUCAGGUCCGUGATT);
629 siRabaptin5 (5'CCGGGCAAUUCUGAAUGAUACUAAA3'); siGGA3
630 (5'CCCGGGUCAUCAACUCUUATT3') or scramble siRNA (siCtrl: non-targeting pre-designed
631 ID 12935112). All siRNAs were purchased from Invitrogen and the silencing experiments were
632 performed 48 hours post transfection.

633

634 **cDNAs and DNA transfection**

635 MCF10A cells were transfected with Lipofectamine 3000 (#L3000075; ThermoFisher
636 Scientific) according to the supplier's instructions. Constructs for Rab4, Rab11 and Rabaptin5
637 were kindly provided from Marino Zerial (MPG Dresden, Germany), and mCherry- and Citrine-
638 tagged ErbB3 were kindly provided by Martin Offterdinger (Innsbruck, Austria). Rabaptin5 was
639 subcloned into pMALC2 (#75286, Addgene) for bacterial expression (see below). mCherry-
640 tagged Rabaptin5 and YFP-tagged Arf6 were purchased from Addgene. Flag-ErbB3 cDNA
641 was subjected to site-directed mutagenesis (Agilent) to generate LL866/7AA mutant Flag-
642 ErbB3. For rescue experiments mCherry-ErbB3 carrying two non-sense point mutations in the
643 siRNA-recognition sequence was subcloned into pAdEasy XL and adenovirus produced using
644 the AdEasy XL adenovirus system (#240010; Agilent) according to the manufacturer's
645 instructions and MCF10A cells infected at a titter that yielded ErbB3 overexpression in
646 approximately 90% of the cells.

647

648 **RT-qPCR**

649 RNA was extracted with the RNeasy Mini Kit (#74104; Qiagen). cDNA was synthesized with
650 the iScript™ cDNA Synthesis Kit (#170-8891; Bio-Rad). qPCR was performed using the KAPA
651 SYBR® Fast and primers for *ERBB3* (5'CAACTCCAGATGAAGACTATG3' and 5'
652 TGCTATGCCAGTAATCAGG3'), *ITGB1* (5'AGATCCGAAGTTTCAAGGGC3' and
653 5'GAACCATGACCTCGTTGTTC3'), *GGA3* (5'GGGACAGGGTGTCTGAGAAAG3' and
654 5'GTGCCTCGTCTTCCTTCACC3'), *RABEP1* (5'TTCCCAGCCTGACGTTTCTC3' and
655 5'GCTGCTGTTGTGCACGTAAA3') and *GAPDH* (5'CCCTTCATTGACCTCAACTA3' and
656 5'CCAAAGTTGTCATGGATGAC3'). The comparative C_t method was used to calculate fold-
657 change in gene expression relative to *GAPDH*.
658

659 **Antibodies**

660 The following primary antibodies were used: anti-ErbB3 (#05-390, clone 2F12, Millipore - for
661 IP, and #12708S, clone D22C5, Cell Signaling Technology - for immunoblotting); anti-Integrin
662 β1 monoclonal (#ab52971, Abcam - for immunoblotting; and #MAB1987Z; clone P4C10,
663 Sigma-Aldrich - for blocking activity). For immunoblotting, we used the antibodies: Anti-
664 phospho-ErbB3 Tyr1289 (#4791, Cell Signaling Technology); anti-EGFR (#2232, Cell
665 Signaling Technology); anti-ErbB2 (#06-562, Millipore); anti-phospho-AKT Thr308 (#2965,
666 Cell Signaling Technology); anti-AKT (#9272, Cell Signaling Technology); anti-phospho
667 ERK1/2 (#9101, Cell Signaling Technology); anti-ERK1/2 (#9102. Cell Signaling Technology);
668 anti-Phosphotyrosine (#05-1050-M; 4G10® Platinum, Millipore); anti-E-cadherin (#610182, BD
669 Transduction Laboratories); anti-Muc1 (#4538, Cell Signaling Technology); anti-Alix (#sc-
670 53540, clone 1A12, SantaCruz Biotechnology); anti-CD81 (#sc-166029, clone B11, SantaCruz
671 Biotechnology); anti-CD63 (#sc-5275, MX-49.129.5, SantaCruz Biotechnology); anti-GM130
672 (#610822, clone 35, BD Biosciences); anti-Rab4A (#610888, BD Biosciences); anti-EDH1
673 (#ab109747, Abcam); anti-Rabaptin5 (#sc-271069, SantaCruz Biotechnology); anti-GGA3
674 (#612311, clone 8, BD Transduction Laboratories); anti-Arf6 (#sc-7971, clone 3A-1, SantaCruz
675 Biotechnology); anti-GAPDH (##2118, clone 14C10, Cell Signaling Technology); anti-α-

676 Tubulin (#T5168, Sigma-Aldrich); anti-β-Actin (#sc-69879, SantaCruz Biotechnology). HRP-
677 conjugated goat anti-mouse (#62-6520), goat anti-rabbit (#65-6120) and rabbit anti-sheep
678 (#31480) secondary antibodies were purchased from ThermoFisher Scientific. Alexa fluor® 594
679 (#A-11037) or Alexa fluor® 488 (#A-11008) conjugated anti-rabbit antibodies (ThermoFisher
680 Scientific) were used for immunofluorescence. For the Integrin β1 recycling assay, we used
681 the Alexa Fluor® 488 anti-human Integrin β1 antibody (#303016, clone TS2/16, Biolegend).
682
683 **Immunoblotting and immunoprecipitation**
684 Cells were lysed in sodium dodecyl sulphate (SDS)-sample buffer (120 mM Tris-HCl pH 6.8, 3
685 % SDS, 15 % glycerol, 0.03 % bromophenol blue, 75 mM dithiothreitol (DTT) and run on 8-
686 10% polyacrylamide gels. Proteins were transferred onto Hybond™-P polyvinylidene fluoride
687 (PVDF) membranes at 100 V for 120 minutes at 4°C. Membranes were blocked in 4% milk or
688 5% bovine serum albumin (BSA), dissolved in TTBS (tris-buffered saline, 0.1% Tween 20).
689 The protein bands were visualized using ECL™ or ECL plus™ reagents and Hyperfilm® ECL
690 (all from GE Healthcare) and detected with a CCD camera (Biorad). Quantification of western
691 blots was performed using the ImageJ software.
692 For ErbB3 immunoprecipitation cells were lysed in: 1% NP40, 50mM Tris HCl pH8.0, 150mM
693 NaCl, 0.5% sodium deoxycholate, 0.1% SDS and 1mM EDTA supplemented with
694 Halt™ phosphatase/protease inhibitor (ThermoFisher Scientific). Preclearing of lysates was
695 performed by incubating samples for 1 hour at 4°C under rotation with Pierce control agarose
696 resin. Antibody incubation was performed overnight 4°C under rotation and precipitates
697 washed 4 times in lysis buffers. Precipitated proteins were resolved by immunoblotting. Arf6
698 immunoprecipitations were performed as above but with lysis buffer: 1% Triton-X100, 100 mM
699 sodium chloride (NaCl), 50mM Tris-HCl pH 7.4. IgG was used as negative control for
700 immunoprecipitations. Immuno-isolation/detection kits coupled to CD63 or CD81 antibodies
701 were purchased from ThermoFisher Scientific (#10606D and #10616D) and used for EV
702 enrichment. The 100K pellets were re-suspended in 100µL PBS with 0.1% BSA (filtered

703 through a 0.2 µm filter) and mixed with 100µL of magnetic beads slurry conjugated to the
704 corresponding antibody according to the manufacturer's instructions.

705

706 **Immunofluorescence**

707 MCF10A or MCF7 cells were cultured on type I bovine collagen (Advanced BioMatrix) coated
708 coverslips and fixed with 4% PFA in PBS for 20 minutes, permeabilized with 0.5% Triton in
709 PBS for 10 minutes and then blocked in Superblock T20 blocking buffer (ThermoFisher
710 Scientific). Primary and secondary antibodies and, where indicated, Alexa fluor® 488-
711 conjugated Phalloidin (ThermoFisher Scientific) were diluted in blocking buffer. Coverslips
712 were mounted using ProLong® Antifade Reagent (ThermoFisher Scientific) with or without
713 DAPI. Images were taken with a Leica SP8 (confocal) or Zeiss Axio Imager M2
714 (epifluorescence) microscopes and processed using Leica Suite or Zeiss ZEN 2011 software,
715 respectively. Images were processed in 8-bit format. Deconvolution of confocal image stacks
716 was carried out in Huygens Essential 19.04 (Scientific Volume Imaging B.V.) using a
717 theoretical PSF, automatic background estimation and CMLE deconvolution algorithm. The
718 final signal to noise ratio was set to 10.

719

720 **Transferrin recycling assay**

721 MCF7 cells were incubated in starvation media supplemented with 25 mM HEPES for 3 hours
722 prior to the assay. Cells were treated with 5 µg/mL of Alexa fluor®-conjugated transferrin
723 (T13343, ThermoFisher Scientific) for 30 minutes on ice. Thereafter, excess of labelled
724 transferrin was removed by three washes with PBS and subsequently incubated in media
725 containing 50 µg/mL unlabelled holo-transferrin (T4132, Sigma-Aldrich) for the indicated times
726 (0, 10, 30, 60 minutes). Finally, the cells were treated with an acidic solution (0.2 M acetic acid
727 and 0.5 M NaCl) for 30 seconds to remove surface labelling, fixed in 4% PFA in PBS for 20
728 minutes at room temperature and mounted. Quantification was performed on tree independent
729 experiments. Mean cell intensity was measured with ImageJ (n>17 images of 1-4 cells for each

730 data point). MCF7 cells were chosen for this assay due to efficient surface-labelling with Alexa
731 fluor®-conjugated transferrin. Attempts to perform the transferrin-recycling assay in MCF10A
732 cells were unsuccessful, due to insufficient surface-labelling with Alexa fluor®-conjugated
733 transferrin in these cells.
734
735 **Integrin recycling assay**
736 MCF10A cells were plated on collagen-coated 24-well plates either sparsely or at high
737 confluency for subsequent scratching. Cells were growth factor-deprived for 3 hours and then
738 put on ice for 5 minutes to cool down. Surface Integrin β1 was labelled at 4°C during 45
739 minutes, then washed twice with PBS and returned to 37°C in order to allow internalisation, as
740 previously described (Arjonen et al. 2012). After 15 minutes, cells were put back on ice and
741 treated for 1 hour with anti-Alexa fluor® 488 (#A11094 ThermoFisher Scientific) in order to
742 quench the remaining surface signal. After quenching, cells were again washed twice with PBS
743 and incubated in deprivation media at 37°C. At indicated times cells were fixed with PFA 4%
744 in PBS for 20 minutes at room temperature. When only Integrin internalisation was monitored,
745 the quenching step was not performed. Quantification of total pixel intensity per cell, mean
746 pixel intensity and average projections were performed with ImageJ.
747
748 **TIRF microscopy**
749 A prism-type TIRF microscope built around a Nikon E600FN upright microscope equipped with
750 a 16× 0.8-NA water-immersion objective was used. The output from diode-pumped solid-state
751 lasers (Cobolt, Stockholm, Sweden) were merged by dichroic mirrors and homogenized and
752 expanded by a rotating, light-shaping diffusor (Physical Optics Corp., Torrance, CA). Excitation
753 light was selected by interference filters (491 nm for Alexa-488 and 561 nm for mRFP, Chroma)
754 mounted in a filter wheel (Lambda 10-3, Sutter Instruments, Novato, CA) and refocused
755 through a modified dove prism (Axicon, Minsk, Belarus) at a 70° angle to achieve total internal
756 reflection. Cells grown on 25-mm glass coverslips (Menzel-Gläser, #1) were kept on ice and
757 mounted in a modified Sykes-Moore perfusion chamber just before imaging, placed on top of

758 the prism and perfused with DMEM/F12 at a rate of 0.1 mL/minute. Emission wavelengths
759 were selected with interference filters (525/25 nm for Alexa 488, 590/20 for mRFP, Chroma)
760 mounter in a filter wheel (Sutter Instruments) and fluorescence was detected by a back-
761 illuminated EM-CCD camera (DU-887, Andor Technology, Belfast, Northern Ireland). Filter
762 wheels and camera were controlled by MetaFluor (Molecular Devices Corp., Downington, PA)
763 and images were acquired every 10 seconds. TIRF penetration depth was 83nm and an
764 electronic shutter prevented light exposure between image captures. Imaging was done at
765 37°C.
766 TIRF microscopy 8-bit images were analysed off-line using ImageJ. Briefly, cell footprints were
767 manually identified and regions of interest covering the edges of the adherent cells were drawn.
768 Intensity changes within these regions through the time course of the experiment (45 minutes)
769 were measured and exported to Excel. All data points were background corrected, followed by
770 normalization to the pre-stimulatory level (F/F0). Cells within large cell clusters were excluded
771 from the analysis.
772
773 **Wound healing assay**
774 MCF10A cells were seeded in Falcon Multiwell 48-well plates and grown to full confluency.
775 Before performing the wound, cells were pre-treated with 1 μM lapatinib or DMSO alone in
776 serum-containing media lacking added growth factors for 1 hour. Thereafter, a scratch was
777 placed in the middle of each well with a sterile pipette tip. After two washes with PBS,
778 lapatinib/DMSO-containing growth-factor deprived but serum containing media was added
779 back to the cells and the wound healing process was monitored using an IncuCyte ZOOM
780 40008 microscope for 14 hours. The obtained images were analysed using the FIJI software.
781
782 **^{35}S-Met/Cys pulse-chase protein turnover assay**
783 MCF10A cells transfected with control or ErbB3 siRNA were incubated with growth factor
784 deprived DMEM media lacking methionine and cysteine supplemented with 10 μCi/mL ^{35}S-
785 methionine/cysteine (Perkin Elmer) for 30 minutes at 37°C. The labelling media was replaced

786 with growth factor deprived MCF10A culture media containing 5 mM L-cysteine and 5 mM L-
787 methionine (Sigma-Aldrich) for the indicated times, prior to cell lysis and immunoprecipitation
788 of Integrin β1, SDS-polyacrylamide (PAGE) gel electrophoresis and detection of incorporated
789 radioactivity using a Phosphoimager. Images were scanned and quantification of three
790 independent experiments was perform in ImageJ.
791
792 **Recombinant protein purification and *in vitro* binding assay**
793 pMalC2-Rabaptin5 was transformed into the BL21S(DE3)pLysS bacterial strain (Invitrogen).
794 Protein expression was induced with 0.3 mM IPTG for 2 hours at 37°C and recombinant MBP-
795 rabaptin5 was purified with an amylose resin (New England Biolabs) according to the
796 manufacturer's instructions and dialysed against lysis buffer (20 mM Tris-HCl pH 7.4, 50 mM
797 NaCl, 0.05 mM PMSF, 6 KIU7/mL aprotinin 0.5 mM DTT, 5% glycerol and 0.5% Triton X-100).
798 Recombinant 6His-ErbB3 was purchased from Sigma. The in vitro binding assay was
799 conducted by incubating 1 µg/mL recombinant ErbB3 with 1 µg/mL recombinant Rabaptin5 in
800 a stringent buffer containing 50 mM Tris, pH 7.5, 150 mM NaCl, 1% NP40, 0.5% sodium
801 deoxycholate, 0.1% SDS, 1 mM EDTA, HALT protease and phosphatase inhibitor overnight at
802 4°C. ErbB3 was immunoprecipitated and bound Rabaptin5 detected by immunoblotting.
803
804 **Colocalisation analysis**
805 Analysis was conducted on confocal fluorescence images and analysed using Image J.
806 Rab4/11 and ErbB3 colocalisation: Single Rab4 or Rab11 positive structures were identified
807 and 40 × 40-pixel squares were drawn with the structures in the centre and saved as separate
808 images. For each cell, a minimum of 15 structures were randomly selected and the intensity
809 of the centre (7-pixel diameter circle, a) and the adjacent volume (background, b) for each
810 structure was determined using ImageJ. These regions were subsequently transferred to the
811 other channel (ErbB3) and similar measurements were performed. The relative enrichment of
812 ErbB3 at the Rab-positive structures was determined by the formula (a-b)/b. An average for
813 each cell was determined, and a minimum of 16 cells was analysed for each condition. Images

814 shown in the paper are average projections of all structures from all cells analysed. ErbB3 and
815 Integrin β1colocalisation: Deconvoluted confocal image stacks were processed into maximum
816 intensity projections using Fiji ImageJ. Signal intensities along manually drawn lines were
817 obtained using the histogram tool. Colocalisation was analysed in image J as enrichment of
818 Integrin β1 in ErbB3 positive structures (as described for ErbB3 and Rab colocalisation above).
819

820 **VSV-G trafficking assay**

821 VSV-G ts045-GFP was expressed in MCF10A cells for 24 hours. Cells were incubated at 40°C
822 for 6 hours, which causes misfolding and trapping of VSV-G in the ER. The cells were then
823 shifted to permissive temperature (32°C) and either PFA-fixed at indicated times for
824 immunofluorescence imaging or subjected to incubation on ice with Sulfo-NHS-SS-Biotin
825 (ThermoFisher Scientific) to biotinylate all surface proteins. Biotinylated cells were lysed in 1%
826 Triton X-100 containing lysis buffer followed by pulldown with Streptavidin-agarose beads
827 (Sigma) overnight and western blot analysis with indicated antibodies.
828

829 **EdU incorporation assay**

830 EdU incorporation into DNA of MCF10A monolayers subjected to a scratch assay in the
831 presence of 1 μM lapatinib or vehicle alone was detected using the Click-iT EdU Alexa-488
832 Fluor Imaging kit (Invitrogen) following the manufacturer's instructions. Cells were later fixed,
833 double stained with DAPI and mounted for microscopic imaging with a Zeiss Axio Imager M2.
834 Quantification of EdU-positive cells at the indicated times in control or ErbB3-silenced cells
835 was performed with ImageJ.
836

837 **EV isolation and characterization**

838 EV isolation and characterization was performed as previously described (Rodrigues-Junior et
839 al. 2019; Théry et al. 2006). The cells were incubated for 48 hours in DMEM/F12 supplemented
840 without horse serum as described above. The serum-free conditioned medium was centrifuged

841 at 1,200 × g for 5 minutes to clear cell debris while measuring the corresponding number of
842 cells. The medium supernatant was filtered through a 0.2 μm filter, was further concentrated
843 20× by tangential flow filtration on a 50 kDa Ultra-15 Centrifugal Filter (Amicon;
844 Merck/Millipore) by centrifugation at 1,200 × g for 30 minutes, and defined as the VSF. EVs
845 smaller than 200 nm were sub-fractionated based on the presence of the tetraspanin CD81
846 protein. VSF (150 μl) was incubated with 40 μL of anti-CD81-magnetic Dynabeads™
847 (#10616D, ThermoFisher Scientific) in 100 μl of 0.2 μm filtered PBS, respectively, for 60
848 minutes at 37°C. The magnetic beads containing CD81-EVs were immobilized, washed with
849 PBS and the isolated EVs were stored at -20°C for up to 30 days. Additionally, conditioned
850 media derived from MCF10A cells were first centrifuged at 1,200 × g to remove cell debris,
851 and subsequently filtered through a 0.2 μm-filter (Sarstedt) and transferred to a polypropylene
852 ultracentrifuge tube (Beckman Coulter). Ultracentrifugation (UC) was carried out for 2 hours at
853 100,000 × g and 4°C degrees in a swinging bucket rotor (SW28, Beckman Coulter).
854 Nanoparticle number and size distribution were measured through NTA (NanoSight system;
855 Malvern Panalytical, equipped with a 532 nm laser and the NTA 3.4 analytic software). Three
856 videos of 60 seconds each were recorded of each sample, using the following settings: camera
857 level 8 and detection threshold 10. The system was calibrated with polystyrene beads of
858 100nm (Malvern). Modal diameter and per cell ratio of nanoparticles were analysed
859 statistically.

860 Transmission electron microscopy preparation was performed on freshly purified VSF or UC
861 enriched EVs. The EVs were mixed with an equal volume of 4% w/v formaldehyde and further
862 incubated with uranyl oxalate, pH 7.0, for 5 minutes, then stained in a drop containing 4% w/v
863 uranyl acetate and 2% w/v methylcellulose on ice and protected from light for 10 minutes, as
864 described (Rodrigues-Junior et al. 2019). Excess of UA/MC was removed by blotting on filter
865 paper.

866 For immuno-gold staining, after the first 3 washes on PBS the protocol follows as indicated:
867 sample was transferred to drops of 50mM Glycine in PBS for 3 × 1 minute. Then the sample

868 was transferred to a drop of blocking solution, 1 % BSA in PBS, for 20 minutes. Primary and
869 secondary incubations were carried out in 0.1% BSA in PBS for 40 minutes and washed away
870 in 0.1 % BSA in PBS for 5 × 1 minute. Sample was then processed for TEM contrasting as
871 described above. Dried grids were examined by TEM (FEI Tecnaii G2) operated at 80kV with
872 an ORIUS SC200 CCD camera and Gatan Digital Micrograph software (Gatan Inc/Blue
873 Scientific).
874
875 **Cell viability assay**
876 Cell viability was quantified using PrestoBlue Cell Viability Reagent (ThermoFisher Scientific)
877 following the manufacturer's instructions. Briefly, 3×10^3 MCF10A cells were seeded into
878 96-well plates and incubated at 37˚C for 24 hours. Then, $1x10^9$ nanoparticles/mL of VSF
879 enriched from cells transfected with siCtrl or siErbB3 was added to each well. Upon 48 hours
880 of treatment, 10 µl of PrestoBlue reagent was added to each well and fluorescence (540 nm
881 excitation/ 590 nm emissions) was measured. The fluorescence units from VSF treated cells
882 were normalized relative to those of vehicle-treated (EV-free media) and the graphs show
883 average values of % viability with standard error of the mean (SEM) of at least three biological
884 experiments.
885
886 **Matrigel invasion assay**
887 Transwell inserts (#351152) for 24-well plates (6.5 mm diameter, 8 µm pore) were coated with
888 300 µg/mL Matrigel matrix (#734-0269; Corning) diluted in coating buffer (10 mM Tris, pH 8.0,
889 0.7% w/v NaCl) and incubated at 37°C for 1 hour. MCF10A cells (5×10^4) treated for 48 hours
890 with VSF (1×10^9 nanoparticles/mL) enriched from cells transfected with siCtrl or siErbB3, or
891 with EV free media (as control), in the absence or presence of IgG or Integrin β1 blocking
892 antibody P4C10 (5 µg/mL), were seeded in DMEM/F12 in the upper chamber, while
893 DMEM/F12 complete media was placed in the lower chamber and incubated at 37°C to induce
894 the invasion through the Matrigel barrier for 16 hours. After incubation, the inserts were fixed
895 in methanol and stained with 4′,6-diamidino-2-phenylindole (DAPI; Sigma-Aldrich). Nuclei were

896 counted in at least five pictures per insert, taken with the 20× objective, using ImageJ. Data
897 were expressed as the percentage of invasion based on the ratio of the mean number of cells
898 invading through Matrigel matrix per mean number of cells in the uncoated permeable support.
899
900 **Protein-protein interaction network analysis**
901 A protein–protein interaction network for proteins interacting with GGA3 was constructed using
902 the Search Tool for the Retrieval of Interacting Genes database (STRING-version 12.0;
903 http://string-db.org/), with the required high confidence score (> 0.7).
904
905 **Statistical analyses**
906 All data, unless otherwise pointed out, are presented as the mean ± SEM, from the indicated
907 independent biological experiments performed in triplicate or quintuplicate technical repeats.
908 Comparisons were performed using two-tailed paired Student's t-test or one-way ANOVA,
909 followed by multiple paired comparisons conducted by means of Bonferroni's post-test method
910 when applicable. Additional statistical methods are explained in the respective figure legends.
911 The data were analysed with GraphPad Prism 10.1 (GraphPad Software, San Diego, CA). A
912 p-value <0.05 was necessary to determine statistically significant differences.
913
914 **Online Supplemental Material**
915 Supplementary Figure S1. ErbB3 promotes Integrin β1 endocytic recycling.
916 Supplementary Figure S2. ErbB3 promotes endocytic recycling of Integrin β1 in absence of
917 EGFR or ErbB2.
918 Supplementary Figure S3. ErbB3 gene expression correlates with BRCA patient survival and
919 chemotherapy response.
920 Supplementary Figure S4. ErbB3 does not affect exocytic trafficking of VSV-G but reduces EV
921 release.
922 Supplementary Figure S5. ErbB3 enhances Integrin β1 stability and binds to GGA3 and
923 Rabaptin5 in vitro.

References

Arjonen, A., J. Alanko, S. Veltel, and J. Ivaska. 2012. Distinct recycling of active and inactive β1 integrins. *Traffic*. 13:610–625. https://doi.org/10.1111/j.1600-0854.2012.01327.x.

Al-Akhrass, H., T. Naves, F. Vincent, A. Magnaudeix, K. Durand, F. Bertin, B. Melloni, M.-O. Jauberteau, and F. Lalloué. 2017. Sortilin limits EGFR signaling by promoting its internalization in lung cancer. *Nat. Commun*. 8:1182. https://doi.org/10.1038/s41467-017-01172-5.

Al-Akhrass, H., J.R.W. Conway, A.S.A. Poulsen, I. Paatero, J. Kaivola, A. Padzik, O.M. Andersen, and J. Ivaska. 2021. A feed-forward loop between SorLA and HER3 determines heregulin response and neratinib resistance. *Oncogene*. 40:1300-1317. doi: 10.1038/s41388-020-01604-5.

Avraham, R. and Y. Yarden. 2011. Feedback regulation of EGFR signalling: decision making by early and delayed loops. *Nat. Rev. Mol. Cell Biol*. 12:104–117. https://doi.org/10.1038/nrm3048.

Bridgewater, R.E., J.C. Norman, and P.T. Caswell. 2012. Integrin trafficking at a glance. *J. Cell Sci.* 125:3695–3701. https://doi.org/10.1242/jcs.095810.

Cao, Z., X. Wu, L. Yen, C. Sweeney, and K.L. Carraway. 2007. Neuregulin-induced ErbB3 downregulation is mediated by a protein stability cascade involving the E3 ubiquitin ligase Nrdp1. *Mol. Cell. Biol*. 27:2180–2188. https://doi.org/10.1128/MCB.01245-06.

Caswell, P.T., M. Chan, A.J. Lindsay, M. W. McCaffrey, D. Boettiger, and J.C. Norman. 2008. Rab-coupling protein coordinates recycling of alpha5beta1 integrin and EGFR1 to promote cell migration in 3D microenvironments. *J. Cell Biol*. 183:143–155. https://doi.org/10.1083/jcb.200804140.

Caswell, P.T., S. Vadrevu, and J.C. Norman. 2009. Integrins: masters and slaves of endocytic transport. *Nat. Rev. Mol. Cell Biol*. 10:843–853. https://doi.org/10.1038/nrm2799.

Christoforides, C., E. Rainero, K.K. Brown, J.C. Norman, and A. Toker. 2012. PKD controls αvβ3 integrin recycling and tumor cell invasive migration through its substrate Rabaptin-5. *Dev. Cell*. 23:560–572. https://doi.org/10.1016/j.devcel.2012.08.008.

Crupi, M.J.F., S.M. Maritan, E. Reyes-Alvarez, E.Y. Lian, B.D. Hyndman, A.N. Rekab, S. Moodley, C.N. Antonescu, and L.M. Mulligan. 2020. GGA3-mediated recycling of the RET receptor tyrosine kinase contributes to cell migration and invasion. *Oncogene*. 39:1361–1377. https://doi.org/10.1038/s41388-019-1068-z.

de Franceschi, N., H. Hamidi, J. Alanko, P. Sahgal, and J. Ivaska. 2015. Integrin traffic - the update. *J. Cell Sci*. 128:839–852. https://doi.org/10.1242/jcs.161653.

de Renzis, S., B. Sönnichsen, and M. Zerial. 2002. Divalent Rab effectors regulate the sub-compartmental organization and sorting of early endosomes. *Nat. Cell Biol*. 4:124–133. https://doi.org/10.1038/ncb744.

Deneka, M., M. Neeft, I. Popa, M. van Oort, H. Sprong, V. Oorschot, J. Klumperman, P. Schu, and P. van der Sluijs. 2003. Rabaptin-5alpha/rabaptin-4 serves as a linker between rab4 and gamma(1)-adaptin in membrane recycling from endosomes. *EMBO J*. 22:2645–2657. https://doi.org/10.1093/emboj/cdg257.

Diamonti, A.J., P.M. Guy, C. Ivanof, K. Wong, C. Sweeney, and K.L. Carraway. 2002. An RBCC protein implicated in maintenance of steady-state neuregulin receptor levels. *Proc. Natl. Acad. Sci. U. S. A.* 99:2866–2871. https://doi.org/10.1073/pnas.052709799.

969 Dietrich, M., M.S. Malik, M. Skeie, V. Bertelsen, and E. Stang. 2019. Protein kinase C
970 regulates ErbB3 turnover. *Exp. Cell Res*. 382:111473.
971 https://doi.org/10.1016/j.yexcr.2019.06.018.

972 Do, M.T., T.F. Chai, P.J. Casey, and M. Wang. 2017. Isoprenylcysteine
973 carboxylmethyltransferase function is essential for RAB4A-mediated integrin β3 recycling,
974 cell migration and cancer metastasis. *Oncogene*. 36:5757–5767.
975 https://doi.org/10.1038/onc.2017.183.

976 Fekete, J.T. and B. Győrffy. 2019. ROCplot.org: Validating predictive biomarkers of
977 chemotherapy/hormonal therapy/anti-HER2 therapy using transcriptomic data of 3,104
978 breast cancer patients. *Int. J. Cancer*. 145:3140–3151. https://doi.org/10.1002/ijc.32369.

979 Fosdahl, A.M., M. Dietrich, K.O. Schink, M.S. Malik, M. Skeie, V. Bertelsen, and E. Stang.
980 2017. ErbB3 interacts with Hrs and is sorted to lysosomes for degradation. *Biochim. Biophys.*
981 *Acta*. 1864:2241–2252. https://doi.org/10.1016/j.bbamcr.2017.08.011.

982 Gaborit, N., M. Lindzen, and Y. Yarden. 2016. Emerging anti-cancer antibodies and
983 combination therapies targeting HER3/ERBB3. *Hum. Vaccines Immunother*. 12:576–592.
984 https://doi.org/10.1080/21645515.2015.1102809.

985 Ghossoub, R., F. Lembo, A. Rubio, C.B. Gaillard, J. Bouchet, N. Vitale, J. Slavík, M.
986 Machala, and P. Zimmermann. 2014. Syntenin-ALIX exosome biogenesis and budding into
987 multivesicular bodies are controlled by ARF6 and PLD2. *Nat. Commun*. 5:3477.
988 https://doi.org/10.1038/ncomms4477.

989 Haskins, J.W., D.X. Nguyen, and D.F. Stern. 2014. Neuregulin 1–activated ERBB4 interacts
990 with YAP to induce Hippo pathway target genes and promote cell migration. *Sci. Signal*.
991 7(355):ra116. https://doi.org/10.1126/scisignal.2005770.

992 Hirschberg, K., C.M. Miller, J. Ellenberg, J.F. Presley, E.D. Siggia, R.D. Phair, and J.
993 Lippincott-Schwartz. 1998. Kinetic Analysis of Secretory Protein Traffic and Characterization
994 of Golgi to Plasma Membrane Transport Intermediates in Living Cells. *J. Cell Biol*. 143:1485–
995 1503.

996 Hoshino, A., B. Costa-Silva, T.-L. Shen, G. Rodrigues, A. Hashimoto, M. Tesic Mark, H.
997 Molina, S. Kohsaka, A. Di Giannatale, S. Ceder, et al. 2015. Tumour exosome integrins
998 determine organotropic metastasis. *Nature*. 527:329–335.
999 https://doi.org/10.1038/nature15756.

1000 Ivaska, J. and J. Heino, J. 2011. Cooperation between integrins and growth factor receptors
1001 in signaling and endocytosis. Annu. Rev. *Cell Dev. Biol*. 27:291–320.
1002 https://doi.org/10.1146/annurev-cellbio-092910-154017.

1003 Jura, N., N.F. Endres, K. Engel, S. Deindl, R. Das, M.H. Lamers, D.E. Wemmer, X. Zhang,
1004 and J. Kuriyan. 2009. Mechanism for activation of the EGF receptor catalytic domain by the
1005 juxtamembrane segment. *Cell*. 137:1293. https://doi.org/10.1016/j.cell.2009.04.025.

1006 Lánczky, A. and B. Győrffy. 2021. Web-Based Survival Analysis Tool Tailored for Medical
1007 Research (KMplot): Development and Implementation. J. *Med. Internet Res*. 23:e27633.
1008 https://doi.org/10.2196/27633.

1009 Lauand, C., P. Rezende-Teixeira, B.A. Cortez, E.L. de O. Niero, and G.M. Machado-Santelli.
1010 2013. Independent of ErbB1 gene copy number, EGF stimulates migration but is not
1011 associated with cell proliferation in non-small cell lung cancer. *Cancer Cell Int*. 13:38.
1012 https://doi.org/10.1186/1475-2867-13-38.

1013 Li, J., B.A. Ballif, A.M. Powelka, J. Dai, S.P. Gygi, and V.W. Hsu. 2005. Phosphorylation of
1014 ACAP1 by Akt regulates the stimulation-dependent recycling of integrin beta1 to control cell
1015 migration. *Dev. Cell*. 9:663–673. https://doi.org/10.1016/j.devcel.2005.09.012.

1016 Lindsay, A.J., A.G. Hendrick, G. Cantalupo, F. Senic-Matuglia, B. Goud, C. Bucci, and M.W.
1017 McCaffrey. 2002. Rab coupling protein (RCP), a novel Rab4 and Rab11 effector protein. *J.*
1018 *Biol. Chem*. 277:12190–12199. https://doi.org/10.1074/jbc.M108665200.

1019 Littlefield, P., L. Liu, V. Mysore, Y. Shan, D.E. Shaw, and N. Jura. 2014. Structural analysis
1020 of the EGFR/HER3 heterodimer reveals the molecular basis for activating HER3 mutations.
1021 *Sci. Signal*. 7:ra114. https://doi.org/10.1126/scisignal.2005786.

1022 Lolo, F.-N., D.M. Pavón, A. Grande-García, A. Elosegui-Artola, V.I. Segatori, S. Sánchez, X.
1023 Trepat, P. Roca-Cusachs, and M.A. Del Pozo. 2022. Caveolae couple mechanical stress to
1024 integrin recycling and activation. *eLife*. 11:e82348. https://doi.org/10.7554/eLife.82348.

1025 Luhtala, S., S. Staff, A. Kallioniemi, M. Tanner, and J. Isola. 2018. Clinicopathological and
1026 prognostic correlations of HER3 expression and its degradation regulators, NEDD4-1 and
1027 NRDP1, in primary breast cancer. *BMC Cancer*. 18(1):1045. doi: 10.1186/s12885-018-4917-
1028 1.

1029 Maretzky, T., A. Evers, W. Zhou, S.L. Swendeman, P.-M. Wong, S. Rafii, K. Reiss, and C.P.
1030 Blobel. 2011. Migration of growth factor-stimulated epithelial and endothelial cells depends
1031 on EGFR transactivation by ADAM17. *Nat. Commun*. 2:229.
1032 https://doi.org/10.1038/ncomms1232.

1033 Mattera, R., C.N. Arighi, R. Lodge, M. Zerial, and J.S. Bonifacino. 2003. Divalent interaction
1034 of the GGAs with the Rabaptin-5-Rabex-5 complex. EMBO J. 22, 78–88.
1035 https://doi.org/10.1093/emboj/cdg015.

1036 Miaczynska, M. and D. Bar-Sagi. 2010. Signaling endosomes: seeing is believing. *Curr.*
1037 *Opin. Cell Biol*. 22:535–540. https://doi.org/10.1016/j.ceb.2010.05.007.

1038 Miller, G.J., R. Mattera, J.S. Bonifacino, and J.H. Hurley. 2003. Recognition of accessory
1039 protein motifs by the gamma-adaptin ear domain of GGA3. *Nat. Struct. Biol*. 10:599–606.
1040 https://doi.org/10.1038/nsb953.

1041 Moreno-Layseca, P., J. Icha, H. Hamidi, and J. Ivaska. 2019. Integrin trafficking in cells and
1042 tissues. *Nat Cell Biol*. 21:122-132. doi: 10.1038/s41556-018-0223-z.

1043 Muralidharan-Chari, V., J. Clancy, C. Plou, M. Romao, P. Chavrier, G. Raposo, and C.
1044 D'Souza-Schorey. 2009. ARF6-regulated shedding of tumor cell-derived plasma membrane
1045 microvesicles. *Curr. Biol*. 19(22):1875–1885. https://doi.org/10.1016/j.cub.2009.09.059.

1046 Nader, G.P.F., E.J. Ezratty, and G.G. Gundersen. (2016). FAK, talin and PIPKIγ regulate
1047 endocytosed integrin activation to polarize focal adhesion assembly. *Nat. Cell Biol*. 18:491–
1048 503. https://doi.org/10.1038/ncb3333.

1049 Ocana, A., F. Vera-Badillo, B. Seruga, A. Templeton, A. Pandiella, and E. Amir. 2013. HER3
1050 overexpression and survival in solid tumors: a meta-analysis. *J Natl Cancer Inst*. 105(4):266-
1051 273. doi: 10.1093/jnci/djs501.

1052 Parachoniak, C.A., Y. Luo, J.V. Abella, J.H. Keen, and M. Park. 2011. GGA3 functions as a
1053 switch to promote Met receptor recycling, essential for sustained ERK and cell migration.
1054 *Dev. Cell*. 20:751–763. https://doi.org/10.1016/j.devcel.2011.05.007.

1055 Pagano, A., P. Crottet, C. Prescianotto-Baschong, and M. Spiess. 2004. In vitro formation of
1056 recycling vesicles from endosomes requires adaptor protein-1/clathrin and is regulated by
1057 rab4 and the connector rabaptin-5. *Mol. Biol. Cell*. 15:4990–5000.
1058 https://doi.org/10.1091/mbc.E04-04-0355.

1059 Pellinen, T. and J. Ivaska. 2006. Integrin traffic. *J. Cell Sci*. 119:3723–3731.
1060 https://doi.org/10.1242/jcs.03216.

1061 Pradeep, S., S.W. Kim, S.Y. Wu, M. Nishimura, P. Chaluvally-Raghavan, T. Miyake, C.V.
1062 Pecot, S.-J. Kim, H.J. Choi, F.Z. Bischoff, et al. 2014. Hematogenous metastasis of ovarian

1063 cancer: rethinking mode of spread. *Cancer Cell*. 26:77–91.
1064 https://doi.org/10.1016/j.ccr.2014.05.002.

1065 Puertollano, R. and J.S. Bonifacino. 2004. Interactions of GGA3 with the ubiquitin sorting
1066 machinery. *Nat. Cell Biol*. 6:244–251. https://doi.org/10.1038/ncb1106.

1067 Qu, F., D.N. Lorenzo, S.J. King, R. Brooks, J.E. Bear, and V. Bennett. 2016. Ankyrin-B is a
1068 PI3P effector that promotes polarized α5β1-integrin recycling via recruiting RabGAP1L to
1069 early endosomes. *eLife*. 5:e20417. https://doi.org/10.7554/eLife.20417.

1070 Qiu, X.-B., and A.L. Goldberg. 2002. Nrdp1/FLRF is a ubiquitin ligase promoting
1071 ubiquitination and degradation of the epidermal growth factor receptor family member,
1072 ErbB3. *Proc. Natl. Acad. Sci. U. S. A*. 99:14843–14848.
1073 https://doi.org/10.1073/pnas.232580999.

1074 Raposo, G. and W. Stoorvogel. 2013. Extracellular vesicles: exosomes, microvesicles, and
1075 friends. *J. Cell Biol*. 200:373–383. https://doi.org/10.1083/jcb.201211138.

1076 Ratcliffe, C.D.H., P. Sahgal, C.A. Parachoniak, J. Ivaska, and M. Park. 2016. Regulation of
1077 Cell Migration and β1 Integrin Trafficking by the Endosomal Adaptor GGA3. *Traffic*. 17:670–
1078 688. https://doi.org/10.1111/tra.12390.

1079 Reynolds, A.R., I.R. Hart, A.R. Watson, J.C. Welti, R.G. Silva, S.D. Robinson, G. Da
1080 Violante, M. Gourlaouen, M. Salih, M.C. Jones, et al. 2009. Stimulation of tumor growth and
1081 angiogenesis by low concentrations of RGD-mimetic integrin inhibitors. *Nat. Med*. 15:392–
1082 400. https://doi.org/10.1038/nm.1941.

1083 Roberts, M., S. Barry, A. Woods, P. van der Sluijs, and J. Norman. 2001. PDGF-regulated
1084 rab4-dependent recycling of alphavbeta3 integrin from early endosomes is necessary for cell
1085 adhesion and spreading. *Curr. Biol*. 11:1392–1402.

1086 Rodrigues-Junior, D.M., S.S. Tan, S.K. Lim, H.S. Leong, M.E. Melendez, C.R.N. Ramos, L.
1087 de S. Viana, D.S.W. Tan, A.L. Carvalho, N.G. Iyer, And A.L. Vettore. 2019. Circulating
1088 extracellular vesicle-associated TGFβ3 modulates response to cytotoxic therapy in head and
1089 neck squamous cell carcinoma. *Carcinogenesis*. 40:1452–1461.
1090 https://doi.org/10.1093/carcin/bgz148.

1091 Sahgal, P., J. Alanko, J. Icha, I. Paatero, H. Hamidi, A. Arjonen, M. Pietilä, A. Rokka, and J.
1092 Ivaska. 2019. GGA2 and RAB13 promote activity-dependent β1-integrin recycling. *J. Cell*
1093 *Sci*. 132: jcs233387. https://doi.org/10.1242/jcs.233387.

1094 Sak, M.M., K. Breen, S.B. Rønning, N.M. Pedersen, V. Bertelsen, E. Stang, and I.H.
1095 Madshus. 2012. The oncoprotein ErbB3 is endocytosed in the absence of added ligand in a
1096 clathrin-dependent manner. *Carcinogenesis*. 33:1031–1039.
1097 https://doi.org/10.1093/carcin/bgs128.

1098 Schlessinger, J. 2002. Ligand-induced, receptor-mediated dimerization and activation of EGF
1099 receptor. *Cell*. 110:669–672.

1100 Smirnova, T., Z.N. Zhou, R.J. Flinn, J. Wyckoff, P.J. Boimel, M. Pozzuto, S.J. Coniglio, J.M.
1101 Backer, A.R. Bresnick, J.S. Condeelis, et al. 2012. Phosphoinositide 3-kinase signaling is
1102 critical for ErbB3-driven breast cancer cell motility and metastasis. *Oncogene*. 31:706–715.
1103 https://doi.org/10.1038/onc.2011.275.

1104 Sönnichsen, B., S. De Renzis, SE. Nielsen, J. Rietdorf, and M. Zerial. 2000. Distinct
1105 membrane domains on endosomes in the recycling pathway visualized by multicolor imaging
1106 of Rab4, Rab5, and Rab11. *J. Cell Biol*. 149:901–914.

1107 Sorkin, A. and L.K. Goh. 2009. Endocytosis and intracellular trafficking of ErbBs. *Exp. Cell*
1108 *Res*. 315, 683–696.

1109 Sun, L., S. Guo, Y. Xie, and Y. Yao. 2023. The characteristics and the multiple functions of
1110 integrin β1 in human cancers. *J. Transl. Med*. 21:787. https://doi.org/10.1186/s12967-023-
1111 04696-1.

1112 Tan, X., N. Thapa, Y. Sun, and R.A. Anderson. 2015. A kinase-independent role for EGF
1113 receptor in autophagy initiation. *Cell*. 160:145–160. https://doi.org/10.1016/j.cell.2014.12.006.

1114 Tang, Z., B. Kang, C. Li, T. Chen, and Z. Zhang. 2019. GEPIA2: an enhanced web server for
1115 large-scale expression profiling and interactive analysis. *Nucleic Acids Res*. 47:W556–W560.
1116 https://doi.org/10.1093/nar/gkz430.

1117 Théry, C., S. Amigorena, G. Raposo, and A. Clayton. 2006. Isolation and characterization of
1118 exosomes from cell culture supernatants and biological fluids. *Curr. Protoc. Cell Biol*.
1119 Chapter 3, Unit 3.22. https://doi.org/10.1002/0471143030.cb0322s30.

1120 Tiwary, S., M. Preziosi, P.G. Rothberg, N. Zeitouni, N. Corson, and L. Xu. 2014. ERBB3 is
1121 required for metastasis formation of melanoma cells. *Oncogenesis*. 3:e110.
1122 https://doi.org/10.1038/oncsis.2014.23.

1123 Tomas, A., C.E. Futter, and E.R. Eden. 2014. EGF receptor trafficking: consequences for
1124 signaling and cancer. *Trends Cell Biol*. 24:26–34. https://doi.org/10.1016/j.tcb.2013.11.002.

1125 van Niel, G., D.R.F. Carter, A. Clayton, D.W. Lambert, G. Raposo, and P. Vader. 2022.
1126 Challenges and directions in studying cell-cell communication by extracellular vesicles. *Nat.*
1127 *Rev. Mol. Cell Biol*. 23:369–382. https://doi.org/10.1038/s41580-022-00460-3.

1128 Wali, V.B., J.W. Haskins, M. Gilmore-Hebert, J.T. Platt, Z. Liu, and D.F. Stern. 2014.
1129 Convergent and Divergent Cellular Responses by ErbB4 Isoforms in Mammary Epithelial
1130 Cells. *Mol. Cancer Res*. 12:1140–1155. https://doi.org/10.1158/1541-7786.MCR-13-0637.

1131 Weaver, V.M., O.W. Petersen, F. Wang, C.A. Larabell, P. Briand, C. Damsky, and M.J.
1132 Bissell. 1997. Reversion of the malignant phenotype of human breast cells in three-
1133 dimensional culture and in vivo by integrin blocking antibodies. *J. Cell Biol*. 137:231–245.
1134 https://doi.org/10.1083/jcb.137.1.231.

1135 Wiley, H.S. 2003. Trafficking of the ErbB receptors and its influence on signaling. *Exp. Cell*
1136 *Res*. 284:78–88.

1137 Woods, A.J., D.P. White, P.T. Caswell, and J.C. Norman. 2004. PKD1/PKCmu promotes
1138 alphavbeta3 integrin recycling and delivery to nascent focal adhesions. *EMBO J*. 23:2531–
1139 2543. https://doi.org/10.1038/sj.emboj.7600267.

1140 Yoshioka, T., Y. Nishikawa, R. Ito, M. Kawamata, Y. Doi, Y. Yamamoto, M. Yoshida, Y.
1141 Omori, H. Kotanagi, T. Masuko, et al. 2010. Significance of integrin αvβ5 and erbB3 in
1142 enhanced cell migration and liver metastasis of colon carcinomas stimulated by hepatocyte-
1143 derived heregulin. *Cancer Sci*. 101:2011–2018. https://doi.org/10.1111/j.1349-
1144 7006.2010.01640.x.

1145 Yu, X., S. Miyamoto, and E. Mekada. 2000. Integrin alpha 2 beta 1-dependent EGF receptor
1146 activation at cell-cell contact sites. *J. Cell Sci*. 113:2139–2147.

1147 Zhai, P., X. He, J. Liu, N. Wakeham, G. Zhu, G. Li, J. Tang, and X.C. Zhang. 2003. The
1148 interaction of the human GGA1 GAT domain with rabaptin-5 is mediated by residues on its
1149 three-helix bundle. *Biochemistry*. 42:13901–13908. https://doi.org/10.1021/bi035392b.

1150 Zhang, R., T. Bu, R. Cao, Z. Li, C. Wang, B. Huang, M. Wei, L. Yuan, and G. Yang. 2022. An
1151 optimized exosome production strategy for enhanced yield while without sacrificing cargo
1152 loading efficiency. *J. Nanobiotechnology*. 20:463. https://doi.org/10.1186/s12951-022-01668-
1153 3.

1154 Zhao, Y. and J.H. Keen. 2008. Gyrating clathrin: highly dynamic clathrin structures involved
1155 in rapid receptor recycling. *Traffic*. 9:2253–2264. https://doi.org/10.1111/j.1600-
1156 0854.2008.00819.x.

1157 Zhu, G., P. Zhai, J. Liu, S. Terzyan, G. Li, and X.C. Zhang. 2004. Structural basis of Rab5-
1158 Rabaptin5 interaction in endocytosis. *Nat. Struct. Mol. Biol*. 11:975–983.
1159 https://doi.org/10.1038/nsmb832.

1160

1161

1162

1163

1164

1165

1166 **FIGURE LEGENDS**

1167 **Figure 1. Ligand-independent role of ErbB3 in epithelial sheet motility**. **(A)** Protein
1168 expression of ErbB3 and GAPDH (as loading control) in the cell extract of MCF10A transiently
1169 transfected with control siRNA (siCtrl) or siRNA targeting ErbB3 (#2). Densitometric values of
1170 ErbB3 protein expression in three biological replicates ± SEM of MCF10A cells is shown
1171 normalized to the respective siCtrl. Data are presented as mean values ± SEM. P-values
1172 determined by unpaired Student's t-test. ** $p \leq 0.01$. (**B**) Scratch closure assay of MCF10A
1173 cells transiently transfected with siCtrl or siErbB3#2, cultured in serum-containing but growth
1174 factor-deprived media in the presence of DMSO (vehicle) or 1 μM of the EGFR/ErbB2 inhibitor
1175 lapatinib. Wound area highlighted in yellow. (**C** and **D**) Quantification of scratch aperture (**C**)
1176 or area under curve (AUC) (**D**) of samples treated as in (**B**). Data are presented as mean
1177 values ± SEM, n-values indicated in parenthesis. (**E**) Quantification of cell proliferation as
1178 incorporation of EdU for the indicated times in control or ErbB3 siRNA#2-transfected cells in
1179 the presence of DMSO (vehicle) or 1 μM lapatinib. Data presented as mean values ± SEM.,
1180 n=3 independent experiments. (**F-I**) Confocal immunofluorescence imaging of surface-labelled
1181 Integrin β1 (green) or actin (blue/black) on confluent sheets of MCF10A cells transfected with
1182 control siRNA (siCtrl) or siErbB3#2 at 0 or 1 hour after labelling (**G**), as outlined in **F**. (**H**) Integrin
1183 β1 enrichment was determined as ((a-b)/b) where a= mean fluorescence intensity (Integrin β1)
1184 at a defined area of the leading edge (**H**) or cell-cell contact (**I**) and b=mean intensity of
1185 adjacent cytoplasm of the same area. Data are presented as mean values (>74 cells per data
1186 point) ± SEM, n=3 independent experiments. Scale bars, 1 mm (**B**) and 10 μm (**G**).

1187

1188 **Figure 2. ErbB3 promotes Integrin β1 and Transferrin receptor endocytic recycling.** (**A-**
1189 **D**) Confocal immunofluorescence imaging of traced surface-labelled Integrin β1 and ErbB3:
1190 MCF7 cells were labelled on ice with an Alexa488-conjugated anti-Integrin β1 antibody prior
1191 to incubation for 15 minutes at 37ºC to allow Integrin β1 internalisation, and subsequent cell-
1192 fixation and immunolabelling of ErbB3 (red) and counterstaining with DAPI (blue). Note that

1193 panel B represents the magnified (squared) regions of panel A. (**C**) Histogram of fluorescence
1194 intensities along dotted lines indicated in **B**. (**D**) Analysis of Integrin β1 and ErbB3
1195 colocalisation. Integrin β1 enrichment in ErbB3-positive intracellular structures (0.5-2 μm
1196 diameter) was determined by the formula (a-b)/b where a is the Integrin β1 intensity at ErbB3
1197 positive structures, and b the adjacent intensity (background) for each structure. Average
1198 intensity projections of all analysed structures are shown on the right-hand side. (**E**) Schematic
1199 outline of Integrin β1 recycling assays conducted in **F-K** after transfection with siRNA against
1200 the indicated targets. Integrin β1 surface-pool was labelled with an Alexa488-conjugated
1201 antibody and allowed to endocytose. Fluorophore label remaining on the cell surface was
1202 quenched with an anti-Alexa488 antibody, prior to visualisation of traced Integrin β1 re-
1203 emerging on the cell surface by live-cell TIRF microscopy. (**F**) Representative TIRF microscopy
1204 images of Integrin β1 from peripheral areas of MCF10A cells transiently transfected with
1205 control siRNA (siCtrl), siErbB3#1 or siErbB3#2. (**G**) Quantifications of recycled Integrin β1
1206 performed on indicated number of cells (outside of brackets on the right-hand side of graphs),
1207 from three independent experiments and shown as Alexa488 intensity normalized between 0-
1208 1, with the control as reference where $F_{norm}=((F_{max}-F_{min})/(F-F_{min}))$. (**H**) Representative TIRF
1209 microscopy images of Integrin β1 from prHMEC cells transiently transfected with siCtrl,
1210 siErbB3#1 or siErbB3#2. (**I**) Quantifications of recycled Integrin β1 in prHMEC performed as
1211 described in E. (**J** and **K**) Quantified Integrin β1 recycling, after siRNA-mediated depletion of
1212 either EGFR (**J**) or ErbB2 (**K**). Data are presented as mean values ± SEM and p-values
1213 determined by two-tailed paired Student's t-test. ns, non-significant. (**L**) Schematic outline of
1214 Transferrin recycling assays. (**M**) Confocal imaging of Alexa594-conjugated Transferrin
1215 chased with unlabelled holo-Transferrin for the indicated times in MCF7 cells. (**N**)
1216 Quantification of Alexa594 fluorescence intensity in cells treated as in **M** (n>17 cells for each
1217 data point from three experiments) normalized against the control siRNA treated, 0-hour
1218 timepoint of each independent experiment. Scale bars, 7 μm (**A), 4** μm **(B), 10** μm **(F, H)** and
1219 **M**) and 0.5 μm (**D**).
1220

1221 **Figure 3. Loss of ErbB3 directs Integrin β1 for secretion as EV cargo.** (**A**) Confocal
1222 imaging of ErbB3-mCherry and indicated Rab marker expressed in MCF10A cells, with or
1223 without prior treatment with the recycling inhibitor primaquine (PQ). (**B**) Analysis of ErbB3-
1224 mCherry colocalisation with Rab4 or Rab11. The relative ErbB3 enrichment at the Rab-positive
1225 structures was determined by the formula (a-b)/b where a is the ErbB3-mCherry intensity of
1226 the centre in Rab4 structures, and b the adjacent volume (background) for each structure.
1227 Each data point represents the minimum average of 20 structures in one cell. P-values were
1228 determined using unpaired two-tailed Student's t-test. (**C**) Average projections of all analysed
1229 (indicated number) GFP-Rab4 or GFP-Rab11 positive structures from the indicated number of
1230 cells (3 independent experiments). (**D**) Experimental outline of the VSV-G trafficking
1231 experiments in MCF10A cells transiently transfected with control siRNA (siCtrl) or siErbB3#2.
1232 (**E**) Immunoblot analysis of the surface pool of VSV-G-ts45-GFP (pulldown of surface-
1233 biotinylated VSV-G-ts45-GFP), after its release from the endoplasmic reticulum (ER) at
1234 permissive temperature for the indicated times. (**F**) Quantification of VSV-G-GFP in biotin-
1235 pulldowns; normalized levels as determined by immunoblot band intensities (n=3 independent
1236 experiments). (**G**) ErbB3 and β-Actin (as loading control) protein expression in MCF10A protein
1237 extracts of wild-type (WT) and transiently transfected cells with the indicated siRNA. (**H**)
1238 Scheme of the EV enrichment protocol by (*i*) ultracentrifugation or (*ii*) tangential flow filtration,
1239 followed by CD81-immunoaffinity capture of EVs from conditioned media of breast epithelial
1240 cells. (**I**) EVs enriched in the VSF released by the indicated MCF10A cells were quantified by
1241 NTA in terms of nanoparticle modal size (nm) and number after normalization to the total cell
1242 number. (**J** and **K**) Protein expression levels of the indicated EV-marker proteins in EV extracts
1243 enriched as VSF (**J**) or CD81-EVs (**K**) derived from MCF10A cells transiently transfected with
1244 the indicated siRNAs; average densitometric values of at least three independent biological
1245 replicates were normalized to siCtrl. **(L)** CD63 protein expression level in EV extracts enriched
1246 by UC derived from MCF10A cells transiently transfected with the indicated siRNAs.
1247 Densitometric quantification of CD63 expression is presented as the mean ± SEM from three
1248 biological replicates, normalized to the corresponding siCtrl condition. (**M**) Rab4A and GAPDH

1249 (as loading control) protein levels in MCF10A cells transiently transfected with the indicated
1250 siRNAs. (**N**) EVs enriched in the VSF released by MCF10A transiently transfected with the
1251 indicated siRNAs were quantified by NTA in terms of nanoparticle modal size (nm) and number
1252 upon normalization to the total cell number. Data presented as mean values ± SEM. P-values
1253 determined by two-tailed paired Student's t-test or one-way ANOVA, followed by multiple
1254 paired comparisons conducted by means of Bonferroni's post-test method. *p ≤ 0.05; **p ≤
1255 0.01; ***p ≤ 0.001; ns, non-significant. Scale bars, 1 μm
1256
1257 **Figure 4. ErbB3 loss directs Integrin β1 towards lysosomal degradation or EV secretion**.
1258 (**A**) Schematic outline of traced internalised Integrin. (**B**) Confocal immunofluorescence
1259 imaging of traced internalised Integrin β1 in MCF10A cells transiently transfected with control
1260 siRNA (siCtrl) or siErbB3#2. (**C**) Quantification of immunofluorescence intensity of internalised
1261 Integrin β1 that was traced for the indicated times after a 15-minute internalisation step (n>32
1262 cells per data point from 5 independent experiments). (**D**) Determination of Integrin β1 turnover
1263 by pulse-chase metabolic labelling: Control or ErbB3 siRNA#1-transfected MCF10A cells were
1264 pulse-chase labelled with radioactive (^{35}S) methionine and cysteine. Radiolabelled Integrin β1
1265 was visualized by radiography of immunoprecipitates (upper panel). Cell lysates and
1266 immunoprecipitates were analysed by immunoblotting. (**E**) Quantification of pulse chased ^{35}S-
1267 labelled Integrin β1 (left panel siErbB3#1 and right panel siErbB3#2) (n=4 independent
1268 experiments). (**F** and **G**) Confocal immunofluorescence imaging of surface-labelled Integrin β1
1269 (using an Alexa488-conjugated anti-Integrin β1 antibody), prior to (0 hour) or after tracing at
1270 37°C for 1.5 hours. A scratch was inflicted prior to antibody incubation. Note that application
1271 of the lysosome inhibitor chloroquine caused Integrin β1 accumulation in intracellular vesicular
1272 compartments both in MCF10A transiently transfected with siCtrl or siErbB3#2. (**H**)
1273 Quantification of Integrin β1 fluorescence intensity in cells bordering the migratory front in
1274 samples treated as in **G**, showing that chloroquine restored Integrin β1 levels in ErbB3-
1275 depleted cells. Data were presented as mean values ± SEM., n=19-27 cells per data point from
1276 3 independent experiments. P-values were determined by two-tailed paired Student's t-test.

1277 ns, non-significant. (**I**) Protein expression of Integrin β1 and the indicated EV-markers in the
1278 UC EV protein extract; average densitometric values of at least three independent biological
1279 replicates were normalized to siCtrl. (**J**) Representative TEM micrographs of EVs enriched by
1280 ultracentrifugation (UC EVs) from control or ErbB3-depleted MCF10A cells and stained with
1281 gold-conjugated anti-CD63 antibody (CD63-EVs are indicated by red arrows). (**K**) Cell viability
1282 assay measured with PrestoBlue Cell Viability Reagent in MCF10A cells transiently transfected
1283 with siCtrl or siErbB3#2 incubated with EV free media as vehicle (Ctrl) or 1×10^9 nanoparticles
1284 of EVs secreted from MCF10A cells transiently transfected with control (VSF^{siCtrl}) or ErbB3-
1285 siRNA ($VSF^{siErbB3}$) for 48 hours. (**L**) Matrigel invasion assay in trans-wells with MCF10A cells
1286 stimulated with EV free media (Ctrl) or incubated with equal number of VSF^{siCtrl} or $VSF^{siErbB3}$ as
1287 described in **K** for 16 hours. (**M**) Matrigel invasion assay in trans-wells with MCF10A WT cells
1288 pre-stimulated for 48 hours with EV free media (Ctrl) or incubated with equal number of VSF^{siCtrl}
1289 or $VSF^{siErbB3}$ in the presence of 5 ug/mL IgG or Integrin β1 monoclonal antibody (mAb; P4C10)
1290 for additional 16 hours. The data in **K-M** are presented as mean values of three biological
1291 replicates ±SEM and p-values shown based on two-way ANOVA, followed by multiple paired
1292 comparisons conducted by means of Bonferroni's post-test method (*$p \leq 0.05$; **$p \leq 0.01$; ***p
1293 ≤ 0.001; ****$p \leq 0.0001$). Scale bars, 15 μm (**A),** 10 μm (**G**), 200nm (**J**).
1294
1295 **Figure 5. ErbB3 scaffolds assembly of the Arf6-GGA3-Rabaptin5 endosomal sorting**
1296 **complex.** (**A**) Immunoblotting of ErbB3 immunoprecipitates or input cell lysates, after 30
1297 minutes treatment with primaquine (PQ), showing endogenous binding of ErbB3 with GGA3
1298 and Rabaptin5 that increases upon PQ treatment, and the presumed accumulation of recycling
1299 endosomes (representative of 3 independent experiments). IgG was used as negative control
1300 for immunoprecipitations. (**B**) Immunoblotting of Arf6 immunoprecipitates or input cell lysates,
1301 transfected with the indicated siRNAs, following PQ or vehicle treatment for 10 minutes. (**C**
1302 and **D**) Quantification of GGA3 and Rabaptin5 protein levels (**C**: immunoblotting) and mRNA
1303 levels (**D**: RT-qPCR) in ErbB3 siRNA-transfected MCF10A cells relative to control cells (n=4
1304 experiments for protein and n=3 for mRNA). Data are presented as mean values ± SEM. P-

1305 values determined by unpaired Student's t-test. (**E**) Structural model highlighting the putative
1306 GGA3-binding motif 864-DxxLL-867 in the ErbB3 kinase domain. (**F**) Immunoblotting of ErbB3
1307 immunoprecipitates or input cell lysates, after ectopic expression of ErbB3 or the ErbB3
1308 LL866/867AA mutant with GGA3 in HEK293T cells. (**G**) The LL866/867AA mutation
1309 compromises the ability of ErbB3 to promote assembly of the Arf6-GGA3-Rabaptin5 sorting
1310 complex: Immunoblotting of Arf6 immunoprecipitates or input cell lysates, following ectopic
1311 expression of Arf6, GGA3 and Rabaptin5, with or without ErbB3 or ErbB3-LL866/867AA.
1312 Average densitometric values of at least two independent biological replicates were normalized
1313 to the respective controls and to the loading control protein when appropriate. **(H)** Confocal
1314 imaging of wild-type (WT) or LL866/7AA mutant ErbB3-mCherry and Alexa594-conjugated
1315 Integrin β1 in MCF10A cells. The analysis of ErbB3-mCherry colocalisation with Integrin β1
1316 shows the relative ErbB3 enrichment at the Integrin β1-positive structures, as determined by
1317 the formula (a-b)/b where a is the ErbB3-mCherry intensity of the centre in Integrin β1
1318 structures, and b the adjacent volume (background) for each structure. Each data point
1319 represents the minimum average of 20 structures in one cell. P-values were determined using
1320 unpaired two-tailed Student's t-test. Scale bars, 15 μm (**H**).
1321
1322 **Figure 6. Rabaptin5 and GGA3 are effectors of ErbB3 in endosomal trafficking.** (**A**)
1323 (**B**) Representative TIRF microscopy images of Integrin β1 from peripheral areas of MCF10A
1324 cells transiently transfected with control siRNA (siCtrl) or siRabaptin5. (**C**) Quantification of
1325 recycled Integrin β1 was conducted on the indicated number of cells (right-hand side of graphs)
1326 from three independent experiments and shown as Alexa488 intensity normalized against
1327 levels at onset of tracing (0) and maximum intensity (1). (**D**) Columns show area under curves
1328 (AUC). (**E**) Determination of Integrin β1 turnover by pulse-chase metabolic labelling. Control
1329 or Rabaptin5 siRNA-transfected MCF10A cells were pulse-chase labelled with radioactive
1330 (^{35}S) methionine and cysteine. Radiolabelled Integrin β1 was visualized by radiography of
1331 Integrin β1 immunoprecipitates (upper panel). Cell lysates and immunoprecipitates were
1332 analysed by immunoblotting as indicated. (**F**) Quantification of radiolabelled Integrin β1 at the

1333 indicated times of three independent pulse and chase experiments. Data are presented as
1334 mean values ± SEM. P-values determined by two-tailed paired Student's t-test. ns, non-
1335 significant. (**G**) Expression of the indicated proteins and GAPDH (as loading control) in the cell
1336 extract of MCF10A cells transiently transfected with siCtrl, siErbB3#2 or siRabaptin5.
1337 Densitometric quantification of the indicated protein expression in MCF10A cells is presented
1338 as the mean ± SEM from three biological replicates, normalized to the corresponding siCtrl
1339 condition. Data are presented as mean values ± SEM. P-values determined by one-way
1340 ANOVA, followed by multiple paired comparisons conducted by means of Bonferroni's post-
1341 test method. *p ≤ 0.05; ** p ≤ 0.01. (**H**) EVs enriched in the VSF released by the indicated
1342 MCF10A transiently transfected with control or Rabaptin5 siRNAs were quantified by NTA in
1343 terms of nanoparticle modal size (nm) and number after normalization to the total cell number.
1344 (**I**) Representative TEM micrographs of EVs enriched in the VSF of control or Rabaptin5-
1345 depleted MCF10A cells (EVs are indicated by red arrows). (**J**) Protein expression in the cell
1346 extract of MCF10A control samples, ErbB3#2- or GGA3-depleted (left panel) of ErbB3, Integrin
1347 β1, GGA3, besides the indicated EV-specific positive (ALIX, TSG101 and CD81) and GAPDH
1348 (as loading control). (**K**) EVs enriched by UC and released by the indicated MCF10A transiently
1349 transfected with control or GGA3 siRNAs were quantified by NTA in terms of nanoparticles
1350 modal size (nm) and number after normalization to the total cell number. Data in **H** and **K** are
1351 presented as mean values ± SEM. P-values were determined by unpaired Student's t-test. *p
1352 ≤ 0.05. (**L**) Protein expression levels of Integrin β1 and the indicated positive and negative EV-
1353 markers in the UC EVs isolated from MCF10A cells described in **I**. Average densitometric
1354 values of at least two independent biological replicates were normalized to siRNA control. (**M**)
1355 Representative TEM micrographs of EVs enriched by UC secreted from control, ErbB3- or
1356 GGA3-depleted MCF10A cells (EVs are indicated by red arrows). Scale bars, 10μm (B),
1357 200nm (**I**), 1μm (**M**).
1358
1359

1360 **Figure 7. Schematic model summarizing the effect of ErbB3 in vesicular trafficking.**
1361 ErbB3, in a ligand-independent manner, engages with Arf6-GGA3-Rabaptin5 endosomal
1362 sorting complex, to promote early recycling of TfR and Integrin β1. Depletion of ErbB3 or its
1363 effectors Rabaptin5 or GGA3 re-routes Integrin β1 from endocytic recycling towards lysosomal
1364 degradation and secretion as EV cargo. Created in BioRender.

1365

1366 **SUPPLEMENTARY FIGURES AND LEGENDS**

1367

1368 **Supplementary Figure S1. ErbB3 promotes Integrin β1 endocytic recycling. (A)** Viability
1369 curves of MCF7 and MCF10A cells in the presence of increasing concentrations of lapatinib
1370 (logarithmic scale) assessed by PrestoBlue fluorescence. Note the lack of significant
1371 differences. **(B)** Protein expression levels of the indicated signaling proteins and GAPDH (as
1372 loading control) in MCF10A cells stimulated with 20 ng/mL EGF in the absence or presence of
1373 1 μM lapatinib for 30 minutes. Average densitometric values of at least two independent
1374 biological replicates were normalized to the respective control condition (EGF-negative;
1375 Lapatinib-positive). **(C)** RT-qPCR analysis of the indicated mRNA levels in MCF7, MCF10A
1376 and prHMEC cells. Values represent fold-change of *ErbB3* (left) and *Integrin β1* (*ITGB1*; right)
1377 mRNA expression relative to *GAPDH*. Data are presented as mean values of three biological
1378 replicates ± SEM, each in technical duplicates. **(D)** Analysis of colocalisation of endogenous
1379 traced Integrin β1, ErbB3 and the recycling endosomal marker EDH1: MCF7 cells were
1380 labelled on ice with an Alexa488-conjugated anti-Integrin β1 antibody (green) prior to
1381 incubation for 30 minutes at 37ºC to allow Integrin β1 internalisation, and subsequent
1382 immunolabelling of ErbB3 (magenta), counterstained for EDH1 (white, right panel). Note that
1383 the squared region in the left panel represents the magnified images of panel **D**. **(E, G)** Protein
1384 expression of ErbB3 and GAPDH (as loading control) in the cell extract of MCF10A (**E**) and
1385 prHMEC (**G**) cells transiently transfected with control siRNA (siCtrl) or two independent siRNAs
1386 targeting ErbB3 (#1 and #2). Densitometric values of ErbB3 protein expression in three

1387 biological replicates ± SEM of MCF10A cells is shown normalized to the respective siCtrl. **(F,**
1388 **H)** Columns show area under curve (AUC) of the Integrin β1 recycling data in MCF10A (**F**:
1389 related to **Figure 2G**) and prHMEC cells (**H**: related to **Figure 2I**). Data presented as mean
1390 values ± SEM, n-values indicated in the main figures. **(I-L)** Immunofluorescence imaging of the
1391 surface pool of Integrin β1 labelled with Alexa488-conjugated antibody on ice for 1 hour, on
1392 MCF10A **(I, J)** or prHMEC cells **(K, L)** transfected with siCtrl or ErbB3-targeting siRNAs. The
1393 columns in **J** and **L** show quantification of Integrin β1 fluorescence intensity, normalized
1394 against control siRNA treated samples. Data presented as mean ± SEM, from 6 independent
1395 experiments. P-values in panels **C**, **E**, **F**, **H**, **J** and **L** were determined by one-way ANOVA
1396 followed by multiple paired comparisons conducted by Bonferroni's post-test method. *p ≤
1397 0.05; **p ≤ 0.01; ***p ≤ 0.001; ****p ≤ 0.0001; ns, non-significant. Scale bars, 10 μm (**D**), 20
1398 μm (**I,K**).
1399
1400 **Supplementary Figure S2. ErbB3 promotes endocytic recycling of Integrin β1 in**
1401 **absence of EGFR or ErbB2. (A)** Immunoblotting analysis of the indicated proteins and α-
1402 Tubulin (as loading control) in the total MCF10A cell lysates under GF-deprived culture
1403 conditions or upon supplementation of the EGF and βNRG, after depletion of ErbB3, EGFR or
1404 ErbB2. **(B)** Immunoblotting analysis of ErbB3, Integrin β1 and GAPDH (as loading control)
1405 upon transfection of prHMEC cells with control or ErbB3 siRNA #1. **(C)** Relative levels of
1406 *Integrin β1* (*ITGB1*) mRNA in MCF10A control or ErbB3 siRNA #1 transfected cells as
1407 determined by RT-qPCR (n=6 independent experiments). Data presented in C are shown as
1408 mean ± SEM. P-value was determined by Mann-Whitney U-test. **(D)** Immunofluorescence
1409 imaging of the surface pool of Integrin β1 labelled with Alexa488-conjugated antibody on ice
1410 for 1 hour, on MCF10A cells transfected with control siRNA (siCtrl) or siRNAs targeting EGFR
1411 or ErbB2. **(E, F)** Quantification of Integrin β1 fluorescence intensity upon silencing of EGFR
1412 **(E)** or ErbB2 **(F)** and normalized against the respective control siRNA-treated samples. Data
1413 presented as mean values ± SEM. **(G)** Live-cell TIRF imaging of MCF10A cells to monitor
1414 recycling of labelled Integrin β1, after prior siRNA-mediated depletion of ErbB2, EGFR or

1415 ErbB3 (#1 and #2). **(H)** Related to the Figures 2J and 2K: shows AUC of the Integrin β1
1416 recycling data. Data presented as mean values ± SEM. n-values indicated in main figures. n-
1417 values indicated in main figures. **(I, J)** Expression of siRNA-resistant ErbB3 restores the
1418 surface pool of traced Integrin β1 in ErbB3-depleted MCF10A cells. **(I)** Confocal imaging of
1419 Integrin β1 labelled on the cell surface with an Alexa488-conjugated antibody, prior to (0 hour)
1420 or after tracing (1 hour), on cells expressing siRNA-resistant mCh-ErbB3 or fluorophore alone
1421 with or without transfection of control (siCtrl) or ErbB3 siRNA as indicated. **(J)** Fluorescence-
1422 intensity (Integrin β1) along cell-cell borders was quantified from 3 independent experiments.
1423 Values were normalized against intensities prior to tracing (0 hour). The results suggest that
1424 off-target effects of the ErbB3 siRNAs do not underlie the observed recycling defect. Data
1425 presented as mean values ± SD, n>230 cell-cell borders from 3 independent experiments and
1426 p values determined by two-tailed paired Student's t-test. **(K)** Immunoblotting analysis of ErbB3
1427 immunoprecipitates or total cell lysates of MCF10A cells cultured in the presence of 5% horse
1428 serum or under growth factor (GF) deprived. Antibodies detecting total phospho-tyrosine
1429 (4G10; pTyr) or the specific phospho-tyrosine 1289 on ErbB3 were used and α-Tubulin was
1430 used as loading control for the total cell lysates. Scale bars, 20 μm (**D,G**), 10 μm (**I**).
1431
1432
1433 **Supplementary Figure S3. ErbB3 gene expression correlates with BRCA patient survival**
1434 **and chemotherapy response. (A)** *ErbB3* mRNA expression levels as log2-transformed
1435 transcripts per million (TPM) in tumor or corresponding normal tissue from TCGA BRCA tumor
1436 vs TCGA normal + GTEx normal datasets was retrieved from the GEPIA2 portal. The data in
1437 the bottom indicates the number (N) of tissue samples analysed in each group and the
1438 differential expression analysis was performed with one-way ANOVA, using disease state as
1439 variable for calculating differential expression. Red *p ≤ 0.01. **(B)** BRCA patient overall survival
1440 was calculated after sample stratification and compared with the Kaplan-Meier plotter
1441 database by auto select cut-off, based on the low and high expression level of *ErbB3* mRNA.
1442 **(C)** BRCA patients were classified as chemotherapy non-responders or responders based on

1443 the relapse-free survival at five years post-treatment. The diagram presents median *ErbB3*
1444 mRNA expression values, along with SEM and minimal and maximal values, as explained in
1445 the table below the graph, which also presents the number (*N*) of analysed patients.
1446 Comparisons were performed using Mann–Whitney U-test (*p ≤ 0.05). **(D)** Representative
1447 protein expression of ErbB3 and GAPDH (as loading control) in the cell extract of MCF7
1448 transiently transfected with control siRNA (siCtrl) or siRNA targeting ErbB3 (#2). **(E)** Confocal
1449 immunofluorescence imaging of traced internalised Integrin β1 in MCF7 cells transiently
1450 transfected with control siRNA (siCtrl) or siErbB3#2. Integrin β1 that was traced for the
1451 indicated times after a 15-minute internalisation step. **(F)** RT-qPCR analysis of *ErbB3* mRNA
1452 levels in MCF7 cells transiently transfected with siRNAs targeting ErbB3 (#2). Values represent
1453 fold-change of *ErbB3* mRNA expression relative to *GAPDH*. Data are presented as mean
1454 values of three biological replicates ± SEM, each in technical duplicates and p-values are
1455 shown based on unpaired Student's t-test. p-values: ****p ≤ 0.0001. Scale bar, 50 μM (**E**).
1456
1457 **Supplementary Figure S4. ErbB3 does not affect exocytic trafficking of VSV-G but**
1458 **reduces EV release. (A)** Immunoblotting analysis of isolated surface-biotinylated VSV-G-ts45-
1459 GFP, following its temperature-dependent release from the endoplasmic reticulum (ER) for 2
1460 hours in MCF10A cells transiently transfected with control siRNA (siCtrl) or siErbB3#2. Note
1461 that ErbB3-depletion does not influence the emergence of VSV-G at the plasma membrane.
1462 **(B)** Confocal imaging of VSV-G-ts45-GFP (green) and markers of the TGN (GM130; blue) and
1463 the cell surface (E-cadherin; magenta) in control or ErbB3 siRNA transfected MCF10A cells at
1464 non-permissive temperature (40°C) and following its subsequent shift to permissive (32°C)
1465 temperature. Note that VSV-G-ts45-GFP localises to the ER at 40°C, while after 30 minutes at
1466 permissive temperature most of the VSV-G-ts45-GFP has moved to the TGN and after 1 hour
1467 to the cell surface, both in the presence or absence of ErbB3. **(C)** Representative TEM
1468 micrographs of EVs enriched in the VSF of control or ErbB3-depleted MCF10A cells (EVs are
1469 indicated by red arrows). **(D)** Representative nanoparticle traces measured by NTA. The VSF
1470 from MCF10A transiently transfected or not (WT) with control siRNA (siCtrl) or independent

1471 ErbB3 siRNAs were analysed by NTA 3.4 software, according to the manufacturer's protocol.
1472 100nm beads were used as a positive control. **(E)** ErbB3 and β-Actin (as loading control)
1473 protein levels in prHMEC cells transiently transfected with the indicated siRNAs. **(F)** EVs
1474 enriched in the VSF released by prHMEC transiently transfected with the indicated siRNAs
1475 were quantified by NTA in terms of nanoparticle modal size (nm) and numbe normalized to the
1476 total cell number. **(G)** ErbB3, Rab4, Integrin β1 and β-Actin (as loading control) protein levels
1477 in MCF7 cells transiently transfected with the indicated siRNAs. **(H)** EVs enriched in the VSF
1478 released by MCF7 transiently transfected with the indicated siRNAs were quantified by NTA in
1479 terms of modal size (nm) and number of nanoparticles, upon normalization to the total cell
1480 number. **(I)** Representative TEM micrographs of EVs enriched in the VSF of control, ErbB3-
1481 depleted or Rab4-depleted MCF7 cells (EVs are indicated by red arrows). Data in panels **F**
1482 and **H** are presented as mean values ± SEM. P-value in panel **F** was determined by unpaired
1483 Student's t-test, while in panel **H** by one-way ANOVA followed by multiple paired comparisons
1484 conducted by Bonferroni's post-test method. *$p \leq 0.05$; *** $p \leq 0.001$; ****$p \leq 0.0001$. Scale
1485 bars, 10 μm **(B)**, 200nm **(C)**, 1 μm **(J).**
1486
1487
1488 **Supplementary Figure S5. ErbB3 enhances Integrin β1 stability and binds to GGA3 and**
1489 **Rabaptin5 in vitro. (A)** Immunoblotting analysis of the indicated proteins and GAPDH (as
1490 loading control) in MCF10A cells, transfected with control (siCtrl) or ErbB3 siRNA #2 prior to
1491 treatment with protein synthesis inhibitor cycloheximide (CHX) or vehicle alone for the
1492 indicated times in hours. **(B)** Quantification of Integrin β1 band intensities presented as mean
1493 values ± SEM, n = 3 independent experiments. **(C)** Protein expression of ErbB3, Integrin β1
1494 and the indicated EV-specific positive (Alix and TSG101) and negative (GM130) markers,
1495 besides α-Tubulin (as loading control) in the cell extract of MCF10A control or ErbB3-depleted
1496 samples. **(D)** Confocal imaging of colocalisation of endogenous ErbB3 with ectopically
1497 expressed mCherry-GGA3 and endogenous Rabaptin5 in MCF7 cells. **(E)** Analysis of ErbB3-
1498 colocalisation with mCherry-GGA3 or Rabaptin5. The relative ErbB3 enrichment at the positive

1499 colocalisation was determined by the formula (a-b)/b where a is the ErbB3 intensity of
1500 mCherry-GGA3 or Rabaptin5 structures centre, and b the adjacent volume (background) for
1501 each structure. Each data point represents the minimum average of 20 structures in one cell.
1502 **(F)** GGA3 protein-protein interaction network analysis using STRING and a confidence score
1503 > 0.7. **(G)** Immunoblotting analysis of MCF10A cells, transfected with control (siCtrl) or ErbB3
1504 siRNA #2 prior to treatment with the proteasome inhibitor MG132 (50 μM) for the indicated
1505 times in hours. MG132 partially restores GGA3 and Rabaptin5 levels in ErbB3-depleted cells.
1506 **(H)** In vitro binding of ErbB3 to Rabaptin5. Immunoblotting of ErbB3-immunoprecipitates
1507 following incubation of recombinant ErbB3 and Rabaptin5. **(I)** Rabaptin5, ErbB3, Integrin β1
1508 and β-Actin (as loading control) protein levels in MCF7 cells transiently transfected with control
1509 siRNA (siCtrl) or siRabaptin5. **(J)** EVs enriched in the VSF released by MCF7 transiently
1510 transfected with siCtrl or siRabaptin5 were quantified by NTA in terms of nanoparticle modal
1511 size (nm) and number upon normalization to the total cell number. **(K)** Representative TEM
1512 micrographs of EVs enriched in the VSF of control or Rabaptin5-depleted MCF7 cells (EVs are
1513 indicated by red arrows). **(L)** Related to **Figure 6J**. Densitometric quantification of the indicated
1514 protein expression in MCF10A cells is presented as the mean ± SEM from three biological
1515 replicates, normalized to the corresponding siCtrl condition. Data are presented as mean
1516 values ± SEM. P-value in panel **B** was determined by two-tailed paired Student's t-test, while
1517 in panel **J** unpaired Student's t-test. P-values in panel **L** was determined by one-way ANOVA
1518 followed by multiple paired comparisons conducted by Bonferroni's post-test method. *p ≤
1519 0.05; ****p ≤ 0.0001. Scale bars, 10 μm **(B)**, 500nm **(C)**

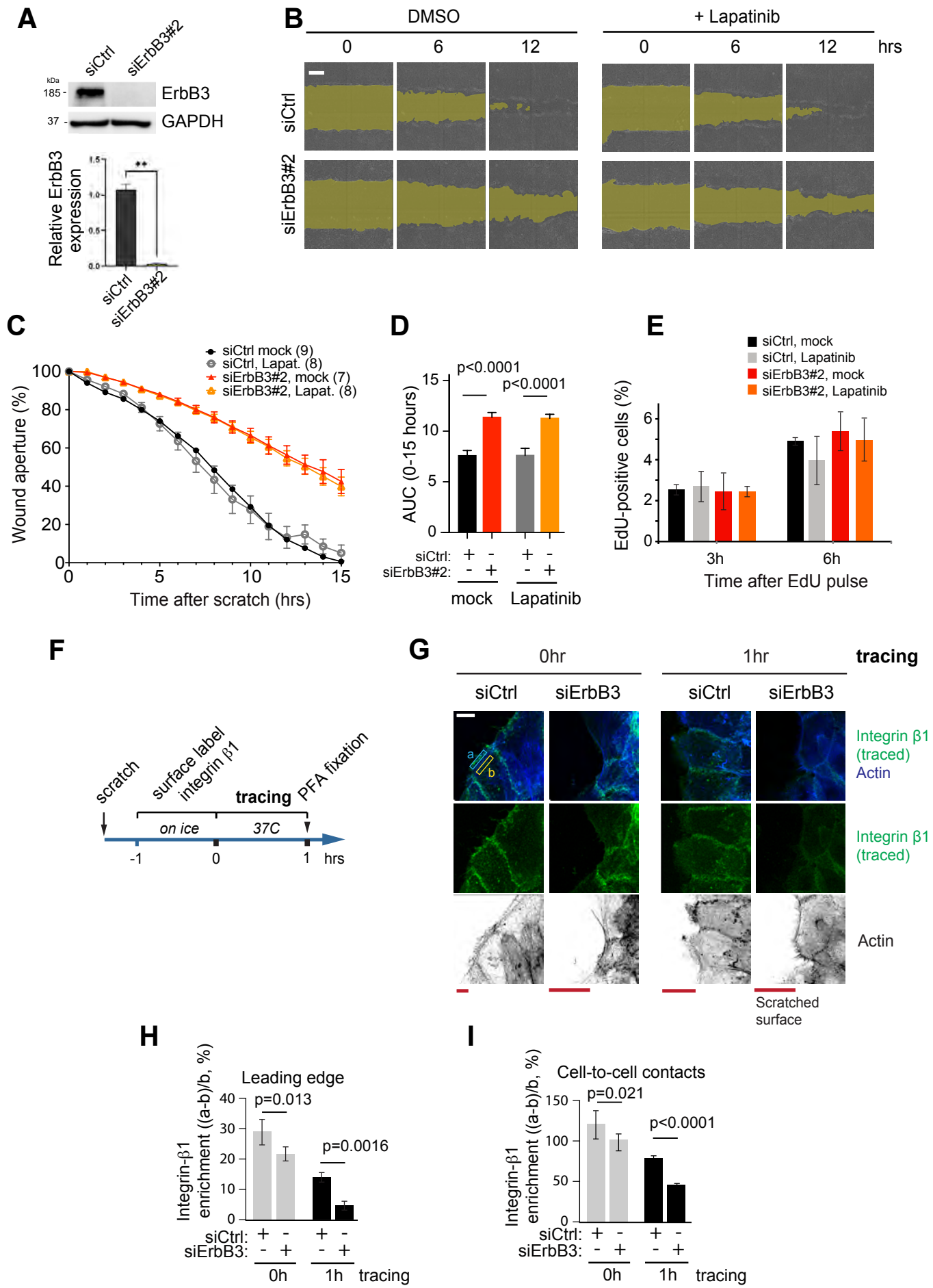
A
siCtrl
siErbB3#2
kDa
185
37
ErbB3
GAPDH
Relative ErbB3 expression
siCtrl
siErbB3#2
B
DMSO
+ Lapatinib
0
6
12
hrs
siCtrl
siErbB3#2
C
siCtrl mock (9)
siCtrl, Lapat. (8)
siErbB3#2, mock (7)
siErbB3#2, Lapat. (8)
Wound aperture (%)
Time after scratch (hrs)
D
p<0.0001
p<0.0001
AUC (0-15 hours)
siCtrl:
siErbB3#2:
mock
Lapatinib
E
siCtrl, mock
siCtrl, Lapatinib
siErbB3#2, mock
siErbB3#2, Lapatinib
EdU-positive cells (%)
3h
6h
Time after EdU pulse
F
scratch
surface label integrin β1
tracing
PFA fixation
on ice
37C
-1
0
1
hrs
G
0hr
1hr
tracing
siCtrl
siErbB3
Integrin β1 (traced)
Actin
Scratched surface
H
Leading edge
Integrin-β1 enrichment ((a-b)/b, %)
p=0.013
p=0.0016
siCtrl:
siErbB3:
0h
1h
tracing
I
Cell-to-cell contacts
p=0.021
p<0.0001

Figure 1

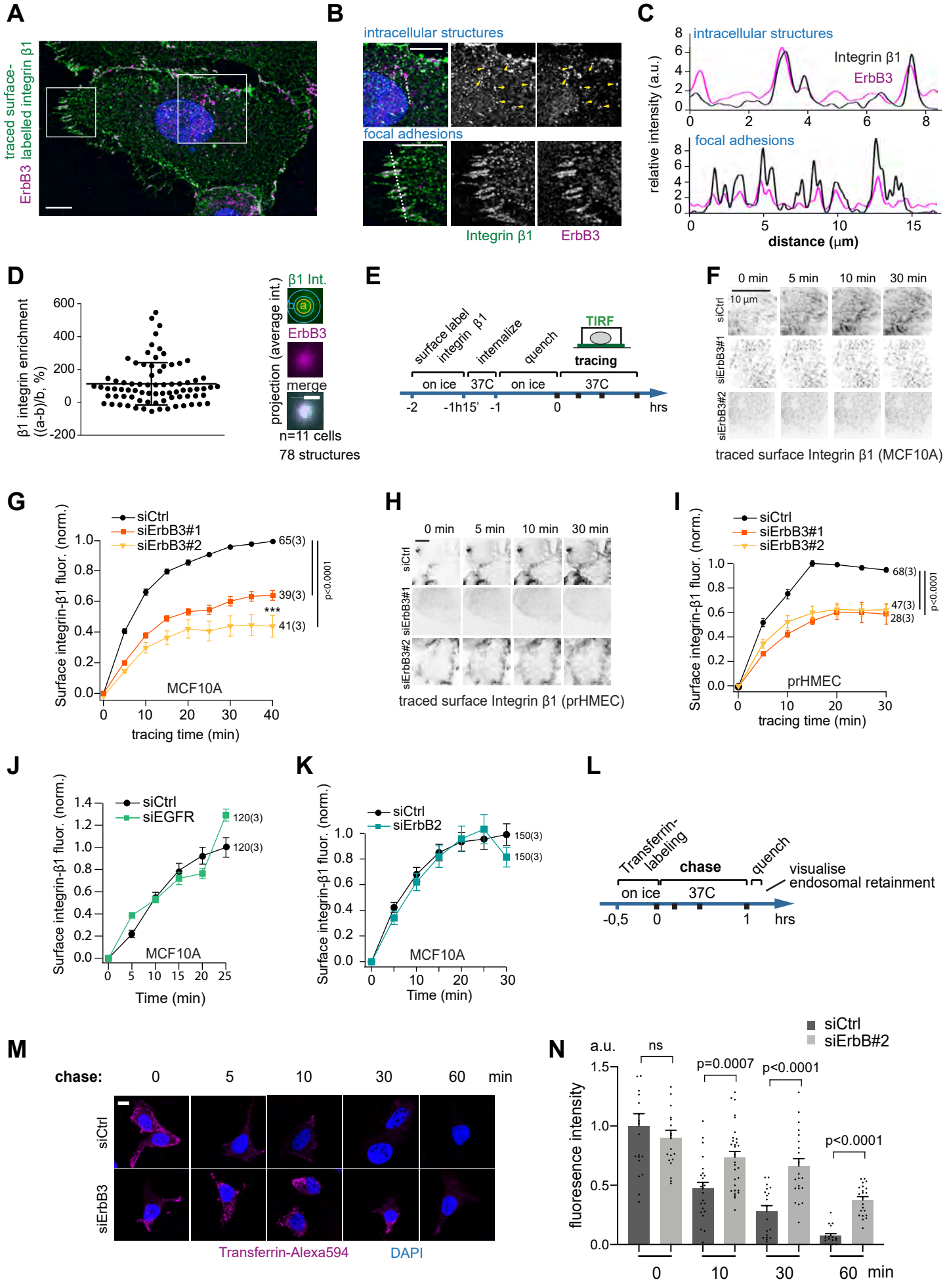
A
traced surface-labelled integrin β1
ErbB3
B
intracellular structures
focal adhesions
Integrin β1
ErbB3
C
intracellular structures
Integrin β1
ErbB3
focal adhesions
relative intensity (a.u.)
distance (μm)
D
β1 integrin enrichment ((a-b)/b, %)
β1 Int.
ErbB3
merge
projection (average int.)
n=11 cells
78 structures
E
surface label integrin β1
internalize
quench
TIRF
tracing
on ice
37C
on ice
37C
-2
-1h15'
-1
0
hrs
F
0 min
5 min
10 min
30 min
10 μm
siCtrl
siErbB3#1
siErbB3#2
traced surface Integrin β1 (MCF10A)
G
siCtrl
siErbB3#1
siErbB3#2
Surface integrin-β1 fluor. (norm.)
65(3)
39(3)
41(3)
***
p<0.0001
MCF10A
tracing time (min)
H
0 min
5 min
10 min
30 min
siCtrl
siErbB3#1
siErbB3#2
traced surface Integrin β1 (prHMEC)
I
siCtrl
siErbB3#1
siErbB3#2
Surface integrin-β1 fluor. (norm.)
68(3)
47(3)
28(3)
p<0.0001
prHMEC
tracing time (min)
J
siCtrl
siEGFR
Surface integrin-β1 fluor. (norm.)
120(3)
120(3)
MCF10A
Time (min)
K
siCtrl
siErbB2
Surface integrin-β1 fluor. (norm.)
150(3)
150(3)
MCF10A
Time (min)
L
Transferrin-labeling
chase
quench
visualise endosomal retainment
on ice
37C
-0,5
0
1
hrs
M
chase:
0
5
10
30
60
min
siCtrl
siErbB3
Transferrin-Alexa594
DAPI
N
siCtrl
siErbB#2
a.u.
fluoresence intensity
ns
p=0.0007
p<0.0001
p<0.0001
0
10
30
60
min

Figure 2

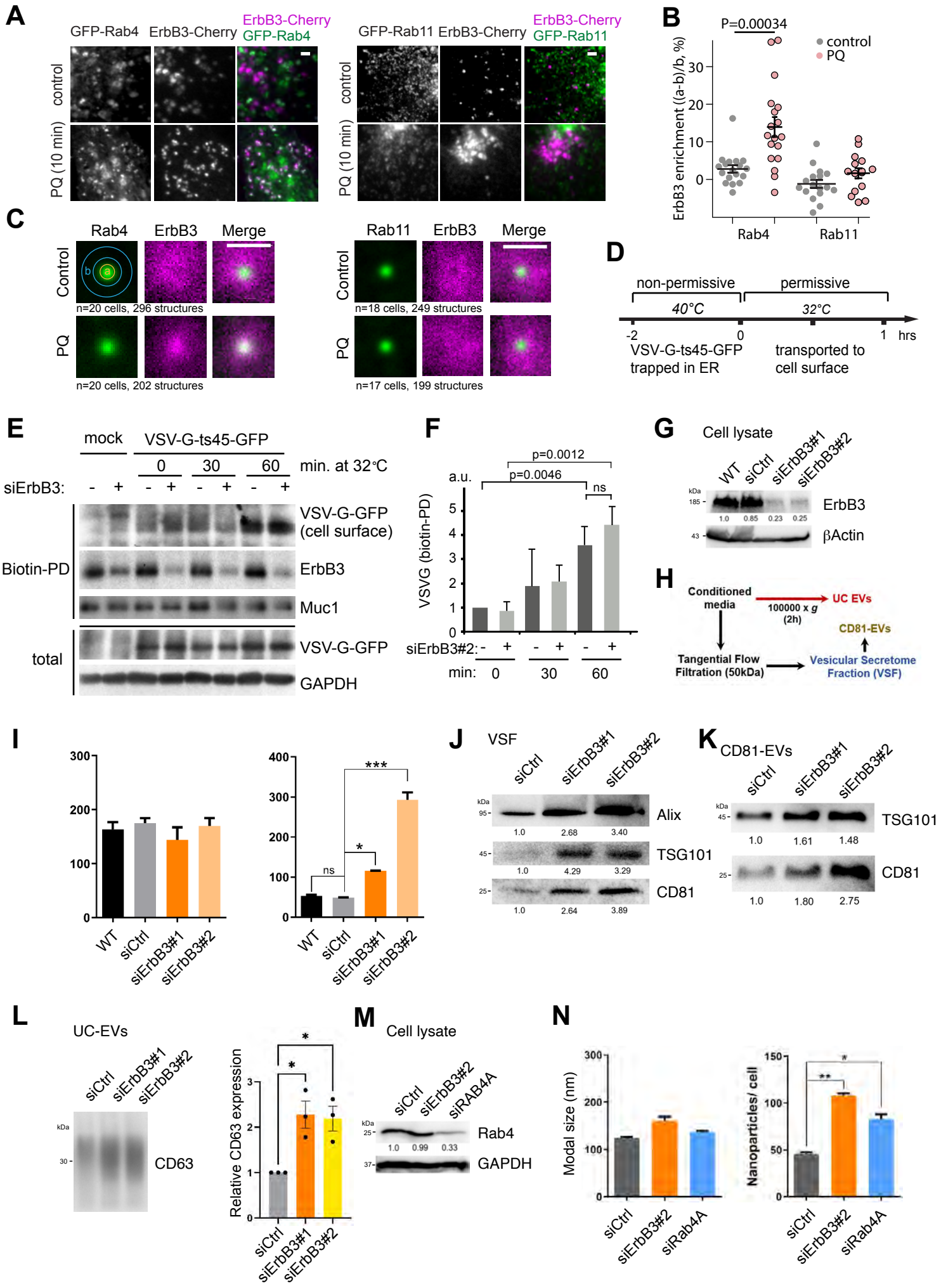
A
GFP-Rab4
ErbB3-Cherry
ErbB3-Cherry GFP-Rab4
GFP-Rab11
ErbB3-Cherry GFP-Rab11
control
PQ (10 min)
B
P=0.00034
control
PQ
ErbB3 enrichment ((a-b)/b, %)
Rab4
Rab11
C
Rab4
ErbB3
Merge
Rab11
Control
PQ
n=20 cells, 296 structures
n=18 cells, 249 structures
n=20 cells, 202 structures
n=17 cells, 199 structures
D
non-permissive
permissive
40°C
32°C
-2
0
1
hrs
VSV-G-ts45-GFP trapped in ER
transported to cell surface
E
mock
VSV-G-ts45-GFP
0
30
60
min. at 32°C
siErbB3:
Biotin-PD
total
VSV-G-GFP (cell surface)
ErbB3
Muc1
VSV-G-GFP
GAPDH
F
a.u.
p=0.0012
p=0.0046
ns
VSVG (biotin-PD)
siErbB3#2:
min:
G
Cell lysate
WT
siCtrl
siErbB3#1
siErbB3#2
ErbB3
βActin
H
Conditioned media
100000 x g (2h)
UC EVs
CD81-EVs
Tangential Flow Filtration (50kDa)
Vesicular Secretome Fraction (VSF)
I
J
VSF
Alix
TSG101
CD81
K
CD81-EVs
TSG101
CD81
L
UC-EVs
CD63
Relative CD63 expression
M
Cell lysate
siRAB4A
Rab4
GAPDH
N
Modal size (nm)
Nanoparticles/ cell
siRab4A

Figure 3

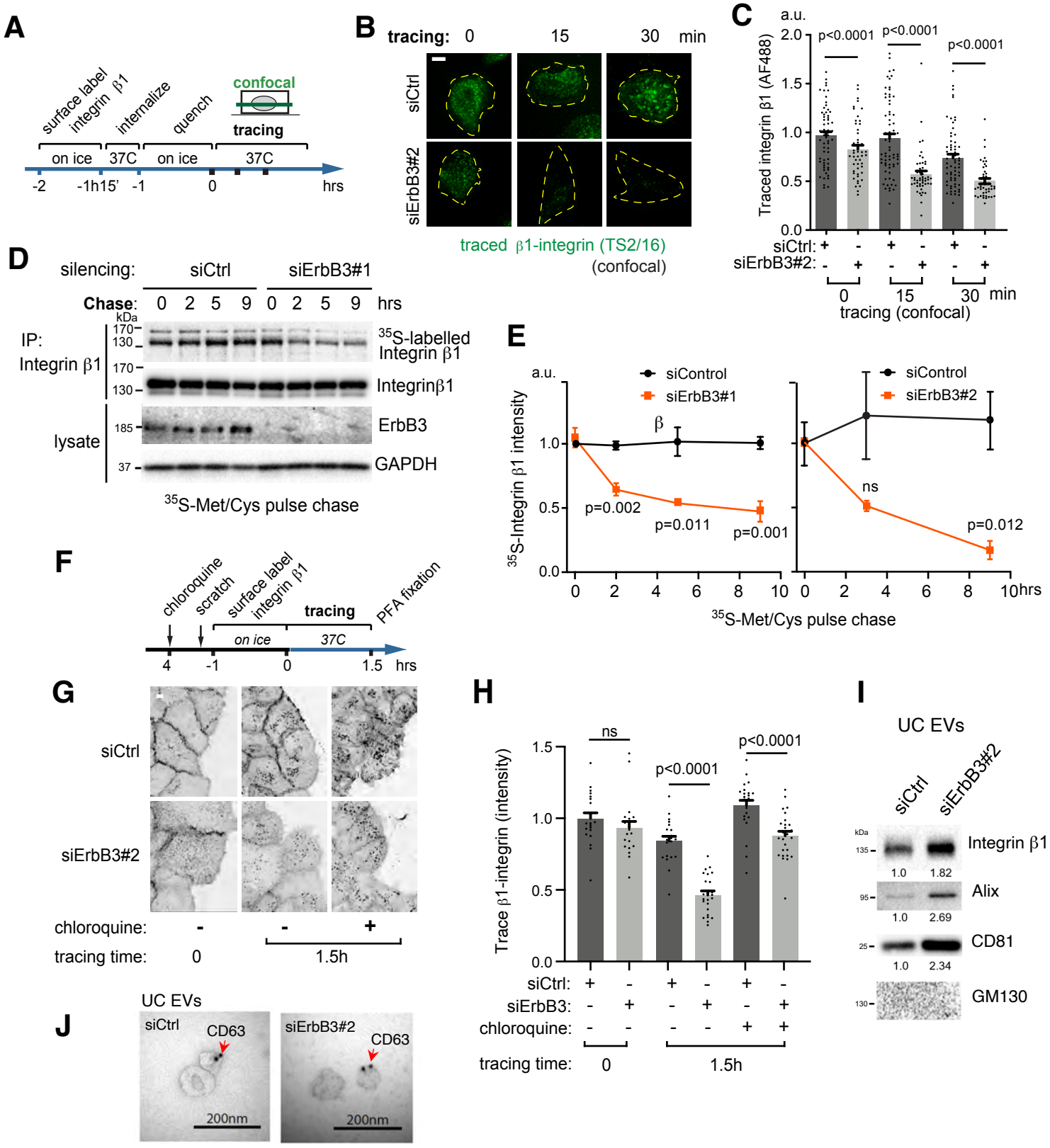
A
surface label integrin β1
internalize
quench
confocal
tracing
on ice
37C
on ice
37C
-2
-1h15'
-1
0
hrs
B
tracing: 0 15 30 min
siCtrl
siErbB3#2
traced β1-integrin (TS2/16) (confocal)
C
a.u.
Traced integrin β1 (AF488)
p<0.0001
p<0.0001
p<0.0001
siCtrl: + - + - + -
siErbB3#2: - + - + - +
0 15 30 min
tracing (confocal)
D
silencing: siCtrl siErbB3#1
Chase: 0 2 5 9 0 2 5 9 hrs
kDa
IP: Integrin β1
35S-labelled Integrin β1
Integrinβ1
lysate
ErbB3
GAPDH
35S-Met/Cys pulse chase
E
a.u.
siControl
siErbB3#1
siErbB3#2
35S-Integrin β1 intensity
β
p=0.002
p=0.011
p=0.001
ns
p=0.012
35S-Met/Cys pulse chase
hrs
F
chloroquine
scratch
surface label integrin β1
tracing
PFA fixation
on ice
37C
4
-1
0
1.5
hrs
G
siCtrl
siErbB3#2
chloroquine: - - +
tracing time: 0 1.5h
H
Trace β1-integrin (intensity)
ns
p<0.0001
p<0.0001
siCtrl: + - + - + -
siErbB3: - + - + - +
chloroquine: - - - - + +
tracing time: 0 1.5h
I
UC EVs
siCtrl
siErbB3#2
Integrin β1
Alix
CD81
GM130
1.0 1.82
1.0 2.69
1.0 2.34
J
UC EVs
siCtrl
siErbB3#2
CD63
200nm
K
Ctrl
VSFsiCtrl
VSFsiErbB3
% Viable cells
siCtrl
siErbB3#2
L
Ctrl
VSFsiCtrl
VSFsiErbB3
% Invasion
siCtrl
siErbB3#2
M
IgG
mAb ITGβ1 (P4C10)
% Invasion
Ctrl
VSFsiCtrl
VSFsiErbB3

Figure 4

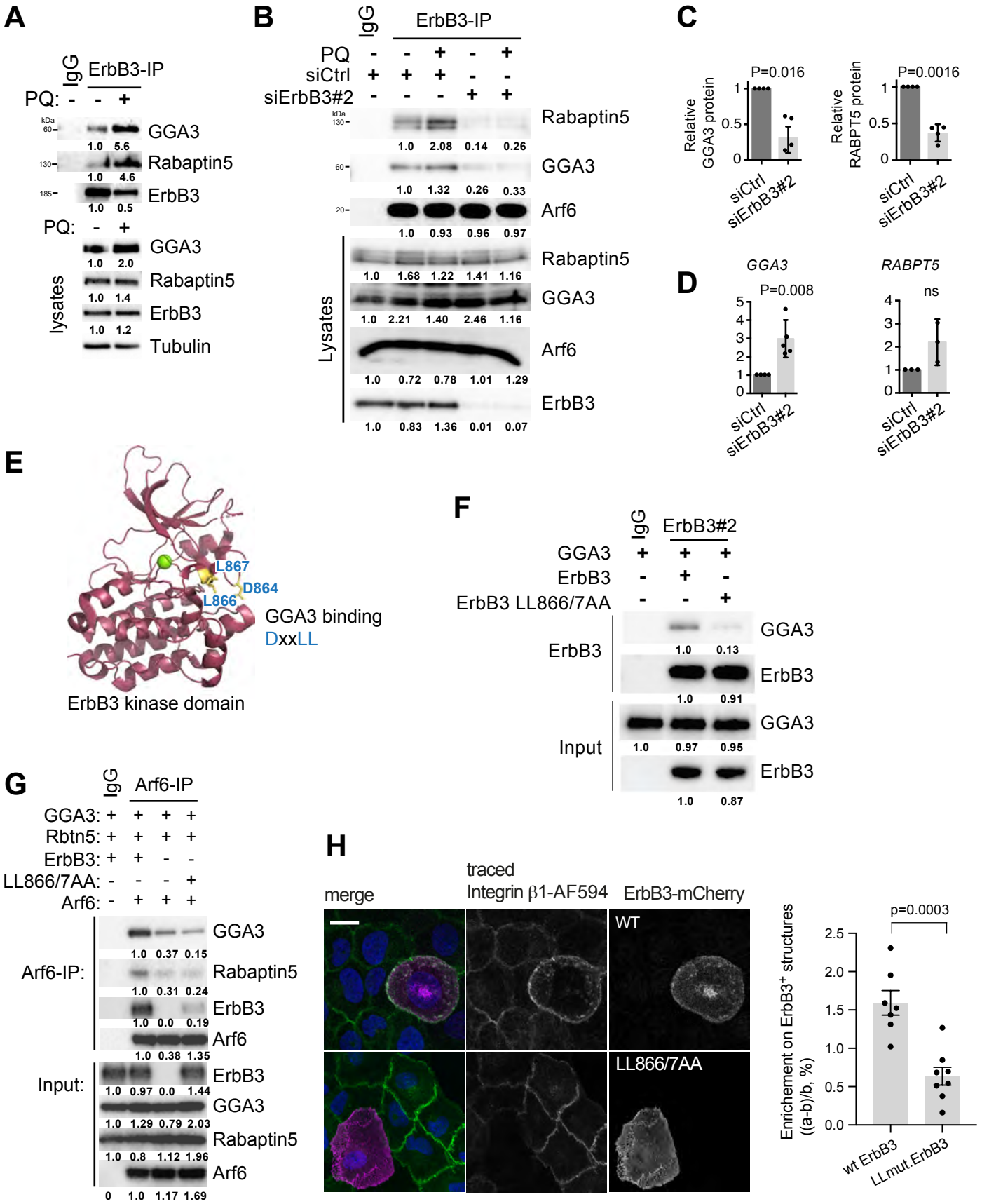
A
IgG
ErbB3-IP
PQ: - - +
kDa
60
GGA3
1.0 5.6
130
Rabaptin5
1.0 4.6
185
ErbB3
1.0 0.5
PQ: - +
GGA3
1.0 2.0
Rabaptin5
1.0 1.4
ErbB3
1.0 1.2
Tubulin
lysates
B
IgG
ErbB3-IP
PQ - - + - +
siCtrl + + + - -
siErbB3#2 - - - + +
kDa
130
Rabaptin5
1.0 2.08 0.14 0.26
60
GGA3
1.0 1.32 0.26 0.33
20
Arf6
1.0 0.93 0.96 0.97
Lysates
Rabaptin5
1.0 1.68 1.22 1.41 1.16
GGA3
1.0 2.21 1.40 2.46 1.16
Arf6
1.0 0.72 0.78 1.01 1.29
ErbB3
1.0 0.83 1.36 0.01 0.07
C
Relative GGA3 protein
P=0.016
siCtrl
siErbB3#2
Relative RABPT5 protein
P=0.0016
siCtrl
siErbB3#2
D
GGA3
P=0.008
siCtrl
siErbB3#2
RABPT5
ns
siCtrl
siErbB3#2
E
L867
D864
L866
GGA3 binding
DxxLL
ErbB3 kinase domain
F
IgG
ErbB3#2
GGA3 + + +
ErbB3 - + -
ErbB3 LL866/7AA - - +
ErbB3
GGA3
1.0 0.13
ErbB3
1.0 0.91
Input
GGA3
1.0 0.97 0.95
ErbB3
1.0 0.87
G
IgG
Arf6-IP
GGA3: + + + +
Rbtn5: + + + +
ErbB3: + + - -
LL866/7AA: - - - +
Arf6: - + + +
Arf6-IP:
GGA3
1.0 0.37 0.15
Rabaptin5
1.0 0.31 0.24
ErbB3
1.0 0.0 0.19
Arf6
1.0 0.38 1.35
Input:
ErbB3
1.0 0.97 0.0 1.44
GGA3
1.0 1.29 0.79 2.03
Rabaptin5
1.0 0.8 1.12 1.96
Arf6
0 1.0 1.17 1.69
H
merge
traced Integrin β1-AF594
ErbB3-mCherry
WT
LL866/7AA
Enrichement on ErbB3+ structures ((a-b)/b, %)
p=0.0003
wt ErbB3
LLmut.ErbB3

Figure 5

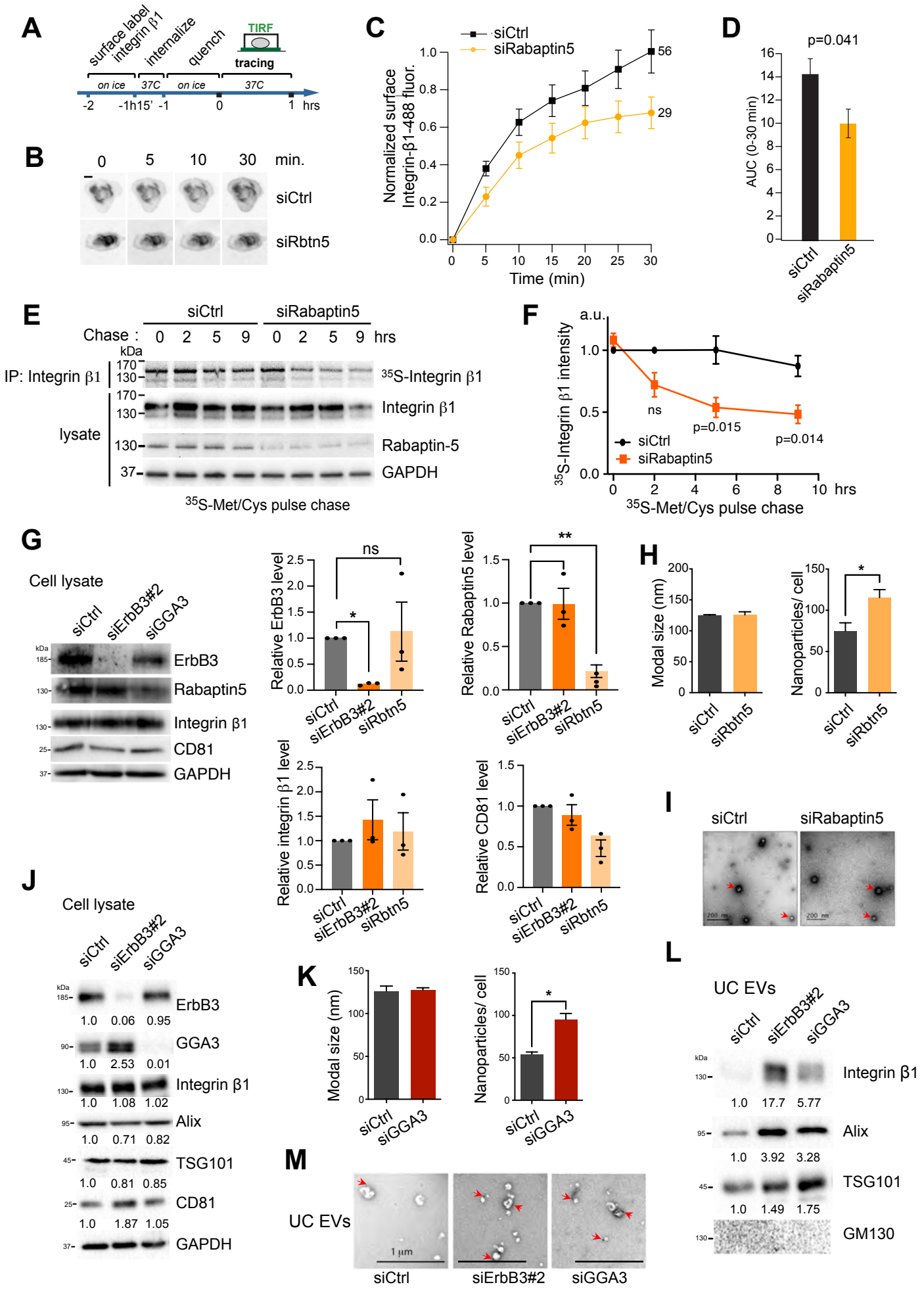
A
surface label integrin β1
internalize
quench
TIRF
tracing
on ice
37C
on ice
37C
-2
-1h15'
-1
0
1
hrs
B
0
5
10
30
min.
siCtrl
siRbtn5
C
siCtrl
siRabaptin5
Normalized surface Integrin-β1-488 fluor.
Time (min)
56
29
D
p=0.041
AUC (0-30 min)
siCtrl
siRabaptin5
E
siCtrl
siRabaptin5
Chase :
0 2 5 9 0 2 5 9 hrs
kDa
IP: Integrin β1
35S-Integrin β1
lysate
Integrin β1
Rabaptin-5
GAPDH
35S-Met/Cys pulse chase
F
a.u.
35S-Integrin β1 intensity
ns
p=0.015
p=0.014
siCtrl
siRabaptin5
hrs
35S-Met/Cys pulse chase
G
Cell lysate
siCtrl
siErbB3#2
siGGA3
ErbB3
Rabaptin5
Integrin β1
CD81
GAPDH
Relative ErbB3 level
Relative Rabaptin5 level
Relative integrin β1 level
Relative CD81 level
ns
H
Modal size (nm)
Nanoparticles/ cell
siCtrl
siRbtn5
I
siCtrl
siRabaptin5
J
Cell lysate
siCtrl
siErbB3#2
siGGA3
ErbB3
1.0 0.06 0.95
GGA3
1.0 2.53 0.01
Integrin β1
1.0 1.08 1.02
Alix
1.0 0.71 0.82
TSG101
1.0 0.81 0.85
CD81
1.0 1.87 1.05
GAPDH
K
Modal size (nm)
Nanoparticles/ cell
siCtrl
siGGA3
L
UC EVs
siCtrl
siErbB3#2
siGGA3
Integrin β1
1.0 17.7 5.77
Alix
1.0 3.92 3.28
TSG101
1.0 1.49 1.75
GM130
M
UC EVs
1 µm
siCtrl
siErbB3#2
siGGA3

Figure 6

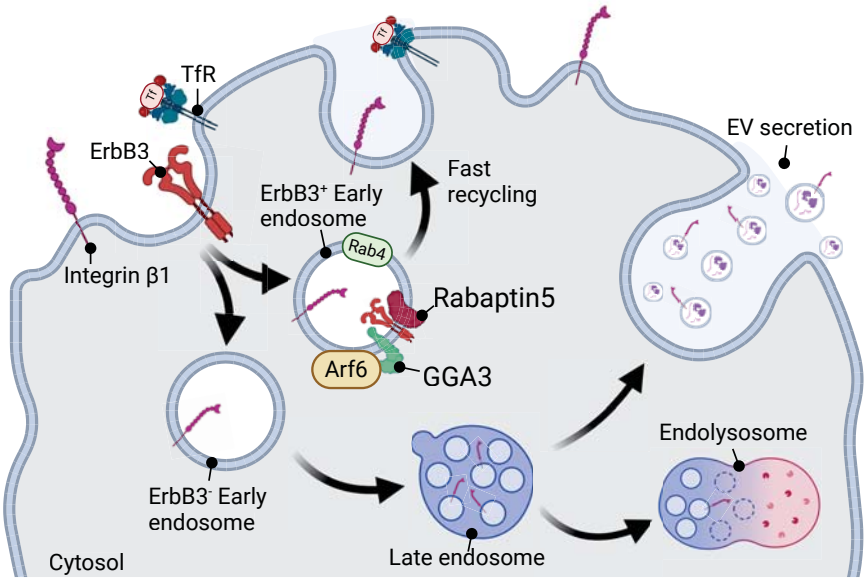
TfR
Tf
ErbB3
Integrin β1
ErbB3⁺ Early endosome
Rab4
Fast recycling
Rabaptin5
Arf6
GGA3
EV secretion
ErbB3⁻ Early endosome
Late endosome
Endolysosome
Cytosol